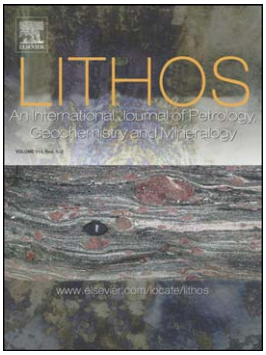

Petrogenesis of meta-volcanic rocks from the Maimón Formation (Dominican Republic): Geochemical record of the nascent Greater Antilles paleo-arc

Lisard Torró, Joaquín A. Proenza, Claudio Marchesi, Antonio Garcia-Casco, John F. Lewis

PII: S0024-4937(17)30053-1
DOI: doi:10.1016/j.lithos.2017.01.031
Reference: LITHOS 4236

To appear in: *LITHOS*

Received date: 19 September 2016
Accepted date: 17 January 2017

Please cite this article as: Torró, Lisard, Proenza, Joaquín A., Marchesi, Claudio, Garcia-Casco, Antonio, Lewis, John F., Petrogenesis of meta-volcanic rocks from the Maimón Formation (Dominican Republic): Geochemical record of the nascent Greater Antilles paleo-arc, *LITHOS* (2017), doi:10.1016/j.lithos.2017.01.031

Petrogenesis of meta-volcanic rocks from the Maimón Formation (Dominican Republic): Geochemical record of the nascent Greater Antilles paleo-arc

Lisard Torró*[,a], Joaquín A. Proenza[a], Claudio Marchesi[b,c], Antonio Garcia-Casco[b,c], John F. Lewis[d]

[a]Departament de Mineralogia, Petrologia i Geologia Aplicada, Facultat de Geologia, Universitat de Barcelona (UB), Martí i Franquès s/n, 08028 Barcelona, Spain

[b]Departamento de Mineralogía y Petrología, Universidad de Granada, Av. Fuentenueva s/n, 18002 Granada, Spain

[c]Instituto Andaluz de Ciencias de la Tierra, CSIC-UGR, Av. de las Palmeras, 4, 18100 Armilla, Granada, Spain

[d]Department of Earth and Environmental Sciences, George Washington University, Washington, DC 20052, USA

Submitted to Lithos

* Corresponding author: Lisard Torró i Abat

Departament de Mineralogia, Petrologia i Geologia Aplicada, Universitat de Barcelona. C/ Martí i Franquès s/n 08028 Barcelona, Catalunya, España

Phone: (+34) 934021344; E-mail: lisardtorro@hotmail.com

Abstract

Metamorphosed basalts, basaltic andesites, andesites and plagiorhyolites of the Early Cretaceous, probably pre-Albian, Maimón Formation, located in the Cordillera Central of the Dominican Republic, are some of the earliest products of the Greater Antilles arc magmatism. In this article, new whole-rock element and Nd-Pb radiogenic isotope data are used to give new insights into the petrogenesis of the Maimón meta-volcanic rocks and constrain the early evolution of the Greater Antilles paleo-arc system. Three different groups of mafic volcanic rocks are recognized on the basis of their immobile element contents. Group 1 comprises basalts with compositions similar to low-Ti island arc tholeiites (IAT), which are depleted in light rare earth elements (LREE) and resemble the forearc basalts (FAB) and transitional FAB-boninitic basalts of the Izu-Bonin-Mariana forearc. Group 2 rocks have boninite-like compositions relatively rich in Cr and poor in TiO_2. Group 3 comprises low-Ti island arc tholeiitic basalts with near-flat chondrite-normalized REE patterns. Plagiorhyolites and rare andesites present near-flat to subtly LREE-depleted chondrite normalized patterns typical of tholeiitic affinity. Nd and Pb isotopic ratios of plagiorhyolites, which are similar to those of Group 1 and 3 basalts, support that these felsic lavas formed by anatexis of the arc lower crust.

Geochemical modelling points that the parental basic magmas of the Maimón meta-volcanic rocks formed by hydrous melting of a heterogeneous spinel-facies mantle source, similar to depleted MORB mantle (DMM) or depleted DMM (D-DMM), fluxed by fluids from subducted oceanic crust and Atlantic Cretaceous pelagic sediments. Variations of subduction-sensitive element concentrations and ratios from Group 1 to the younger rocks of Groups 2 and 3 generally match the geochemical progression from FAB-like to boninite and IAT lavas described in subduction-initiation ophiolites. Group 1 basalts likely formed at magmatic stages transitional between FAB and first-island arc magmatism, whereas Group 2 boninitic lavas resulted from focused flux melting and higher degrees of melt extraction in a more mature stage of subduction. Group 3 basalts probably represent magmatism taking place immediately before the establishment of a steady-state subduction regime. The relatively high extents of flux melting and slab input recorded in the Maimón lavas support a scenario of hot subduction beneath the nascent Greater Antilles paleo-arc. Paleotectonic reconstructions and the markedly depleted, though heterogeneous character of the mantle source, indicate the rise of shallow asthenosphere which had sourced mid-ocean ridge basalts (MORB) and/or back-arc basin basalts (BABB) in the proto-Caribbean domain prior to the inception of SW-dipping subduction. Relative to the neighbouring Aptian-Albian Los Ranchos Formation, we suggest that Maimón volcanic rocks extruded more proximal to the vertical projection of the subducting proto-Caribbean spreading ridge.

Keywords: Forearc, subduction-initiation, ophiolite, Greater Antilles paleo-arc, slab fluids

1. Introduction

Ophiolites are relicts of temporally and spatially associated ultramafic, mafic and felsic rocks which are constituents of oceanic crust and upper mantle emplaced into continental margins through different tectonic mechanisms (Dilek and Furnes, 2014). A number of ophiolite types are classified according to their tectonic setting of formation (Dilek and Furnes, 2014; Pearce, 2014; Pearce and Robinson, 2010) and mode of emplacement (Beccaluva et al., 2004; Moores, 1982; Wakabayashi and Dilek, 2000). Subduction-related or supra-subduction zone ophiolites include those in which oceanic lithosphere formed in the extended upper plate of a subduction zone either in a forearc, arc or back-arc position. Among these, subduction-initiation ophiolites, formed in the forearc during the inception and early stages of intra-oceanic subduction, are those that have been defined most recently (Stern and Bloomer, 1992) and our understanding has developed rapidly in the last decade (e.g., Lázaro et al., 2016; Maffione et al., 2015; Pearce and Robinson, 2010; Pearce et al., 2014; Stern et al., 2012; Turner et al., 2014; Whattam and Stern, 2011). This knowledge has hugely benefitted from the study of *in situ* dredged and drilled basement lithologies of the archetypical Izu-Bonin-Mariana (IBM) forearc (Ishizuka et al., 2011, 2014; Pearce et al, 2015; Reagan et al., 2010; Ribeiro et al., 2013, 2015), which has even led to the definition of a new chemostratigraphic model for subduction initiation magmatism, involving: 1) forearc basalts (FAB; Reagan et al., 2010); 2) boninites and island arc tholeiites (IAT); and 3) island arc tholeiite to calc-alkaline arc magmas. These represent, respectively: 1) initial spreading of oceanic crust above the nascent descending slab and melting of the incipient mantle wedge; 2) fluid-mediated melting of the now-extremely depleted mantle wedge due to addition of large volumes of fluids from hydrated lithosphere; and 3) establishment of a steady-state subduction regime (Ishizuka et al., 2014; Whattam and Stern, 2011). This new subduction initiation paradigm led to the reclassification of many ophiolites previously ascribed to mid-ocean ridge (MOR) or back-arc basin (BAB) settings (cf. Pearce and Robinson, 2010).

Located in the core of the Cordillera Central of the Dominican Republic, the Maimón Formation (Fm.) is one of the oldest Greater Antillean subduction-related volcanic units of the Caribbean island-arc (e.g., Lidiak and Anderson, 2015). Nevertheless, its age is uncertain as attempts to date this unit by geochronological methods have been unsuccessful; a pre-Albian age is inferred by some authors on the basis of geochemical similarity to other IAT and boninite units in the Greater Antilles (Horan, 1995; Lewis et al., 2000, 2002). The tectonic setting and genetic relationship with other arc-related crustal and mantle units in the Cordillera Central are still subject

of debate (e.g., Escuder-Viruete et al., 2007a; Horan, 1995; Nelson et al., 2011; Torró et al., 2016a). Here we present new whole-rock major- and trace-element and Nd-Sr-Pb radiogenic isotope data of metamorphosed volcanic rocks of the Maimón Fm. Our intensive sampling of recently drilled cores has allowed, for the first time, the definition of a clear chemostratigraphic genetical model of these metaigneous rocks, hitherto confused by intense faulting and lack of exposure. Variations of rare earth elements (REE), high field strength elements (HFSE), transition elements and radiogenic isotope ratios in metavolcanic rocks are used (1) to evaluate the composition and the degree of melting of the mantle source and (2) to assess the nature of the slab component involved in the magma genesis through time. In addition, the data are used to better constrain (3) the origin of the Maimón Fm. in the framework of the early Greater Antilles arc, (4) its genetic connections to contiguous arc-related crustal and mantle units and (5) the geometry of initial subduction between the Caribbean and Proto-Caribbean Plates. The proper contextualization of the Maimón Fm. is not a trivial and local question but one that has a major impact in our understanding of the very early evolution of the Caribbean island-arc.

2. Geological setting

2.1. Geodynamic setting

The location and tectonics of the modern Caribbean Plate are the result of (1) the Jurassic breakup and separation of North America and Gondwana, (2) the subsequent progressive west to east insertion of the allochthonous (Pacific-derived) Caribbean Plate into the Atlantic realm, and (3) a collisional event linked to the convergence of the North America and the Caribbean Plates in the latest Cretaceous-earliest Tertiary (Boschman et al., 2014; Lidiak and Anderson, 2015; Pindell et al., 2012, and references therein). The most widespread igneous suites described in the Caribbean are (a) pre-arc basaltic oceanic crust of Jurassic-Early Cretaceous age (Escuder-Viruete et al., 2009; Lidiak and Anderson, 2015; Lidiak et al., 2011; Mattinson et al., 2008; Neill et al., 2010, 2014), (b) Jurassic to Late Cretaceous oceanic plateau rocks of the Caribbean Large Igneous Province (CLIP, which comprises the plume-related Caribbean-Colombian Oceanic Plateau-CCOP) (Kerr et al., 2003; Lidiak and Anderson, 2015, and references therein; Escuder-Viruete et al., 2016), (c) allochthonous Andean/Cordilleran arc rocks (pre-to-syn early Cretaceous volcanic-arc; Blein et al., 2003; Neill et al., 2012; Rojas-Agramonte et al., 2011), and (d) arc-related volcanic and plutonic rocks of Caribbean affinity, which span in age from the Early Cretaceous to the Eocene in the Greater Antilles, and to the present in the Lesser Antilles (Lázaro et al., 2016; Lidiak and Anderson, 2015 and references therein; Rojas-Agramonte et al., 2016). Independently on the initial polarity of the Early Cretaceous subduction (cf. Lidiak and Anderson, 2015), arc-related magmatism initiated

at ca. 135 Ma (Pindell et al., 2012; Rojas-Agramonte et al., 2011). The Early Cretaceous (ca. 135-110 Ma) boninitic and tholeiitic magmatic suites broadly predate the more voluminous calc-alkaline magmatic suite formed in the Late Cretaceous-Eocene time (ca. 95-45 Ma; Lidiak and Anderson, 2015, and references therein). In the Greater Antilles, subduction-related magmatism ceased as a result of arc-continent collision in the northern leading edge of the Caribbean after consumption of Late Jurassic oceanic Proto-Caribbean lithosphere between the Cretaceous arc(s) and the Bahamas platform (Mann et al., 1991). The collision triggered the obduction of ophiolitic complexes onto continental margins in Guatemala, Cuba, Hispaniola and Puerto Rico (Escuder-Viruete et al., 2014; Garcia-Casco et al., 2008a; Lewis et al., 2006; Marchesi et al., 2006, 2011, 2016; Pindell et al., 2012; Solari et al., 2013) and the evolution of the plate margin to the current scenario of left-lateral strike-slip tectonics and oblique convergence between the Caribbean and North America (Mann et al., 2002; Vila et al., 1987).

The island of Hispaniola (Haiti and the Dominican Republic), located in the northern edge of the Caribbean Plate, is a tectonic collage of mantle and crustal units thrusted and uplifted between the Late Eocene and the present (Escuder-Viruete et al., 2008; Lewis and Draper, 1990). Arc- and non-arc-related oceanic units are exposed in central Dominican Republic and are tectonically bounded by the left-lateral strike-slip Hispaniola (HFZ) and San Juan Restauración (SJRFZ) fault zones (Fig. 1a). In the Cordillera Central geological province, transpressional WNW-ESE faults juxtaposed tectonostratigraphic units with different pre-Eocene evolutions, which include: (1) the serpentinized Loma Caribe peridotites (Lewis et al., 2006; Marchesi et al., 2016; Proenza et al., 2007), (2) Late Jurassic MOR gabbros and basalts of the Proto-Caribbean crust (Loma la Monja assemblage), (3) Cretaceous enriched MORB (E-MORB), ocean island basalts (OIB) and picrites, which are onshore representatives of the CLIP (Aptian Duarte complex and Campanian-Maastrichtian Pelona-Pico Duarte and Siete Cabezas formations; Escuder-Viruete et al., 2007b, 2008, 2011) (Fig. 1a), and (4) Cretaceous arc-related igneous and sedimentary rocks (Maimón-Amina, Los Ranchos, Río Verde, Peralvillo and Tireo formations; Escuder-Viruete et al., 2006, 2007a, c, 2010; Lewis et al., 1991, 2000; Torró et al., 2016a).

2.2.The Maimón Formation

The Maimón Fm. is exposed in a 9 km wide and about 73 km long NW-SE trending belt that crops out along the Median Belt of the Dominican Cordillera Central (Fig. 1). The Maimón Fm. is in steep, faulted contact with the Loma Caribe peridotites to the southwest and with the Los Ranchos Fm. to the northeast (Fig. 1b) (Lewis et al., 2002). To the south, the Loma Caribe peridotite belt is separated from the Maimón Fm. by the Peralvillo Sur Fm., a thin sequence of

undeformed and unmetamorphosed arc-related volcanic and volcanosedimentary rocks of Late Cretaceous age (Lewis et al., 2000; Martín and Draper, 1999). The Early Cretaceous volcanic arc rocks of the Maimón and Los Ranchos formations are overlain by the Albian to Cenomanian shallow-water reefal Hatillo limestone (Kesler et al., 1991a, 2005a; Myczynski and Iturralde-Vinent, 2005). The Maimón Fm. overthrusts the Hatillo limestone along the Hatillo Thrust, whose movement is, at least in part, post-Early Eocene (Draper et al., 1996). Both the Maimón and Hatillo formations are intruded by diorite dykes and plugs of Paleocene age (Bowin, 1966; Martín and Draper, 1999).

The Maimón Fm. is composed of bimodal mafic-felsic volcanic and volcaniclastic rocks and a thin belt of well-laminated rocks of sedimentary origin. Sedimentary rocks include fine-grained meta-tuffs, dark graphite-shales, cherts and limestones conformable with the volcanic sequence; they crop out in the northern central part of the Maimón Fm. (Kesler et al., 1991b; Lewis et al., 2000). The volcanic rocks, with boninitic and tholeiitic affinities, are representative of the early island-arc volcanism in the Caribbean region (Fig. 1a) (Escuder-Viruete et al., 2007a; Lewis and Draper, 1990; Lewis et al., 2002; Torró et al., 2016a). Escuder-Viruete et al. (2007a) suggested a cogenetic origin for the Maimón, Amina and Los Ranchos formations. In contrast, Lewis et al. (2000) distinguished a forearc setting for the Maimón and Amina formations and an axial island-arc context for the Los Ranchos Fm. The fact that the Maimón and Amina formations mainly host exhalative sulphide deposits in contrast to the porphyry-epithermal deposits hosted by the Los Ranchos Fm. supports a forearc setting for the former and an arc axis environment for the latter (Nelson et al., 2011; Torró et al., 2016a; Torró et al., *accepted*).

The rocks of the Maimón Fm. are characterized by the development of syn-metamorphic ductile fabrics and structures. As described by Draper et al. (1996) and Draper and Gutiérrez-Alonso (1997), the intensity of ductile deformation and the metamorphic grade increase towards the SW in the Maimón belt, as observed particularly well in the Ozama shear zone (Fig. 1b) that constitutes the upper level of the structural sequence. Deformation and metamorphism, at conditions up to the transition between the greenschists and blueschists facies (Torró et al., 2016b), are much less intense to the NE of the Fátima thrust fault, i.e., in the so-called El Altar zone. Rocks in this zone vary from fully recrystallized to weakly metamorphosed and even slightly undeformed, and a pronounced change in the intensity of metamorphic recrystallization and deformation is observed on each side of the Fátima thrust fault.

3. Material and methods

This study is based on a total of 182 drill core and *in situ* field rock samples representative of the volcanosedimentary material of the Maimón Fm. in its south-central section (ca. from the Hatillo dam to the Ozama River near *el Llano* and *la Majagua*; Fig. 1). A petrographic study previous to ongoing whole-rock geochemical measurements was carried out on 45 thin sections. Rocks of the Ozama shear zone include greenschists and gneissic low-K meta-plagiorhyolites; these samples are pervasively deformed and recrystallized, and lack magmatic remnants. The metamorphic paragenesis mostly includes chlorite, phengite, epidote, amphibole (actinolite ± winchite), albite and quartz, even if the abundance of minerals diverges as a function of bulk-rock composition. Rocks from the El Altar zone are fine-grained plagioclase- and pyroxene-phyric, massive basalts and highly fine- to medium-grained quartz-phyric massive plagiorhyolites that show remarkably less intense ductile deformation and penetrative foliation than rocks of the Ozama shear zone, and limited metamorphic recrystallization. In these samples, phengite and chlorite are the main metamorphic phases along with less abundant epidote and paragonite. More detailed petrographic descriptions and chemical analyses of metamorphic phases are given in Torró et al. (2016b).

Whole-rock geochemistry (Appendix A; selected analyses in Table 1) was determined for a total of 35 samples of (meta-)volcanic rocks that encompass the whole lithological variability of the Maimón Fm. Samples were carefully prepared by removing secondary veins and weathering products before crushing and powdering in an agate mill. Major element and Zr concentrations were determined on glass beads, made up of ~ 0.6 g powdered sample diluted in 6 g of $Li_2B_4O_7$, by a Philips Magix Pro (PW-2440) X-Ray fluorescence (XRF) equipment at the University of Granada (Spain) (Centro de Instrumentación Científica, CIC). Precision was better than ± 1.5% for an analyte concentration of 10 wt. %. Precision for Zr was better than ± 4% at 100 ppm concentration. Trace elements, except Zr, were determined at the University of Granada (CIC) by ICP Mass Spectrometry (ICP-MS) after HNO_3 + HF digestion of ~ 100 mg of sample powder in a Teflon lined vessel at ~ 180 °C and ~ 200 psi for 30 min, evaporation to dryness, and subsequent dissolution in 100 ml of 4 vol.% HNO_3. Procedural blanks and international standards PMS, WSE, UBN, BEN, BR and AGV (Govindaraju, 1994) were run as unknowns during analytical sessions. Precision was better than ± 2% and ± 5% for analyte concentrations of 50 and 5 ppm, respectively. Replicate analyses of international reference materials analysed with our samples are shown in Appendix A.

Neodymium, Sr and Pb radiogenic isotope ratios were measured for whole-rocks. A total of 17 specimens encompassing the whole geochemical lithotypes were selected, including 12 basalts, 2 andesites and 3 plagiorhyolites.

Whole-rock Sr and Nd isotopic analyses were carried out at the CIC of the University of Granada. About 100 mg of powdered rock samples were digested by HNO_3 + HF in Teflon-lined vessels at 200 psi. The elements were separated by ion-exchange resins, and the Sr and Nd isotopic ratios were determined by thermal ionization mass spectrometry (TIMS) in static mode on a Finnigan Mat 262 instrument. All reagents were ultra-clean. Normalization values were $^{86}Sr/^{88}Sr$ = 0.1194 and $^{146}Nd/^{144}Nd$ = 0.7219. Blanks were 0.6 and 0.09 ng for Sr and Nd, respectively. The external precision (2σ), estimated by analysing 10 replicates of the standard WS-E (Govindaraju et al., 1994), was better than 0.0013% for $^{87}Sr/^{86}Sr$ and 0.0019% for $^{143}Nd/^{144}Nd$. The internal precision was estimated by the average of analyses of standards NIST-987 (mean $^{87}Sr/^{86}Sr$ = 0.710249 ± 0.0005%) and La Jolla (mean $^{143}Nd/^{144}Nd$ = 0.511864 ± 0.0011%). $^{87}Rb/^{86}Sr$ and $^{147}Sm/^{144}Nd$ ratios were determined by ICP-MS at the University of Granada, following the method of Montero and Bea (1998). Their precision, estimated by analysing 10 replicates of the standard WS-E, was better than 1.2% and 0.9% (2σ) for $^{87}Rb/^{86}Sr$ and $^{147}Sm/^{144}Nd$, respectively.

Whole-rock Pb isotopic analyses were carried out at the Geochronology and Isotopic Geochemistry General Survey of the University of Basque Country (Spain). For each sample, about 100 mg of powdered rock was digested overnight by HF-HNO_3 and evaporated to dryness. The residue was taken in HBr, and Pb isolated by conventional ion-exchange chromatography (AG1-X8 resin in HBr and HCl media). The recovered lead was evaporated to dryness, dissolved in 0.32N HNO_3 and diluted to a final concentration of 150-200 ppb. Lead isotope ratios were measured by a ThermoNEPTUNE multicollector ICP-MS, and the mass fractionation was internally corrected after the addition of the thallium isotopic reference material NBS-997. Detailed analytical protocols are similar to those described by Chernysev et al. (2007). Accuracy of the results was tested by several analyses of reference material NBS-981, which gave mean ratios of $^{206}Pb/^{204}Pb$ = 16.9425 ± 19, $^{207}Pb/^{204}Pb$ = 15.5006 ± 14, $^{208}Pb/^{204}Pb$ = 36.7270 ± 45, $^{208}Pb/^{206}Pb$ = 2.16774 ± 18, and $^{207}Pb/^{206}Pb$ = 0.91489 ± 6 (n = 4).

4. Results

4.1.Whole-rock major and trace elements

4.1.1. Elemental mobility due to alteration

The (meta-)volcanic rocks of the Maimón Fm. have undergone extensive sea-floor metamorphism that transformed them to spilites and keratophyres, as well as hydrothermal alteration linked to the formation of volcanogenic massive sulphide deposits (Lewis et al., 2000; Torró et al., 2016a). Torró et al. (2016a; see Fig. 3A therein) determined that hydrothermal

alteration included strong chloritization, sericitization, sulphide (pyrite) mineralization and silicification. In addition, the rocks of the Maimón Fm. were metamorphosed to upper greenschist to near-blueschists facies conditions in the case of the Ozama shear zone rocks (Torró et al., 2016b). Under such conditions, most major (Si, K, Na, Ca, Mg, Fe) and large ion lithophile (LILE) elements (Rb, Ba, Sr) are expected to be mobilized; in contrast, high field strength elements (HFSE), rare earth elements (REE) and some transition metals (i.e., Ti, V, Cr) are considered mostly immobile in such post-magmatic conditions (Hastie et al., 2007; Pearce, 2014; Winchester and Floyd, 1977).

Most of the LOI values of the samples in this study are ~ 3 to 5 wt. %, even if values up to 11 wt. % were obtained, evidencing the moderate to strong impact of hydrothermal alteration and metasomatism. Element mobility diagrams (i.e., plots of mobile vs immobile elements for rocks within a cogenetic magmatic suite) show that the concentrations of most mobile elements are scattered in the Maimón (meta-)volcanics, indicating sub-solidus mobilization, whereas immobile elements draw clear magmatic trends (Fig. 2 and Appendix B). Hence, the figures plotted hereinafter, used to classify the samples and infer tectonic constraints, are generally restricted to immobile elements. The samples studied here are classified using the Zr/Ti vs Nb/Y discrimination diagram (Fig. 3a) (Pearce, 1996 after Winchester and Floyd, 1977) into sub-alkaline basalts (20), basaltic andesites (3), andesites (3) and plagiorhyolites (4). Likewise, in the Th vs Co classification diagram (Fig. 3b) (Hastie et al., 2007), the studied rocks classify as basalts, basaltic andesites, andesites and plagiorhyolites of the tholeiite series. The major element contents of the least altered (according petrographic observations and LOI < 3 wt. %) volcanic rocks of the Maimón Fm. define a tholeiitic line of descent in the AFM plot (Fig. 4). The major element concentrations for each rock-type reported below are restricted to the abundances in the least altered samples

4.1.2. Geochemistry of the volcanic rocks

4.1.2.1 Basalts and basaltic andesites

The basalts and basaltic andesites from the Maimón Fm. can be classified into three main groups according to their TiO_2 and Cr (used as immobile proxy for MgO; Pearce, 2014) contents and their normalized REE patterns (Fig. 5).

Group 1 comprise the majority of the studied basalts and basaltic andesites (13 samples), which are characterized by relatively low Cr contents (~ 2-150 ppm) and TiO_2 contents that range between 0.46 and 0.65 wt. %; these values are similar to those of low-Ti tholeiites (LOTI). In chondrite-normalized (CN) REE diagrams (Fig. 5a), Group 1 rocks present N-MORB-like patterns with a strong LREE depletion relative to middle REE (MREE) (La/Sm_{CN} = 0.3-0.6) and heavy REE

(HREE) (La/Yb_{CN} = 0.2-0.5), and flat MREE and HREE segments (Sm/Yb_{CN} = 0.7-1.1). Only three samples show moderate Eu negative anomalies. N-MORB-normalized (NMN) extended trace elements patterns (Fig. 5b) reveal that Group 1 basalts are depleted in immobile trace elements relative to N-MORB and present variable negative Nb (Nb/La_{NMN} = 0.3-1.1) and positive Th (Th/La_{NMN} = 1.4-5.1) anomalies. The extent of subduction component, estimated by the Th/Nb_{NMN} ratio, is low to moderate and varies between 3.2 and 8.0. These compositions are generally more depleted than those of forearc basalts (FAB) from the IBM arc and low-Ti (LOTI) tholeiites from the Los Ranchos Fm. (Escuder-Viruete et al., 2006), and they resemble transitional FAB from the Mariana arc (Fig. 5b).

Group 2 comprises three basalts (including the MMLP 317 sample of Horan, 1995) with higher Cr contents (~ 340-800 ppm) than Group 1, Mg# [100 x molar MgO/(MgO+FeO)] = 63-68, and low TiO_2 (0.28 to 0.46 wt. %), which indicate a boninitic affinity (Pearce, 2014). CN REE patterns (Fig. 5c) are N-MORB-like and are characterized by LREE depletion relative to MREE (La/Sm_{CN} = 0.5-0.8) and HREE (La/Yb_{CN} = 0.4-0.7), and near flat segments for MREE and HREE (Sm/Yb_{CN} = 0.8-0.9). One sample has an evident Eu negative anomaly. NMN extended patterns (Fig. 5d) reveal that immobile trace elements are depleted relative to N-MORB and that the samples have negative Nb (Nb/La_{NMN} = 0.3-0.7) and subtle positive Th (Th/La_{NMN} = 1.6-2.9) anomalies. Their subduction component is moderate (Th/Nb_{NMN} = 4.2-5.6). Group 2 basalts encompass the composition of boninites in the Los Ranchos Fm. and the Mariana arc (Fig. 5d).

Group 3 basalts and basaltic andesites (seven samples) have relatively low Cr contents (~ 2-186 ppm), TiO_2 contents that range between 0.40 and 0.80 wt. %, and Mg# between 50 and 59. Group 3 rocks mainly differ from samples of Group 1 as they show near flat REE normalized patterns (La/Sm_{CN} = 0.7-1.1; La/Yb_{CN} = 0.6-1.2; Sm/Yb_{CN} = 0.8-1.1; Fig. 5e). Three samples present moderate Eu negative anomalies. Their extended normalized patterns (Fig. 5f) show that Group 3 rocks are mildly depleted in immobile trace elements, except Th, but they are in general less depleted than samples of Group 1. Based on the Th contents relative to LREE, Group 3 is subdivided into two subgroups hereafter referred to as 3i and 3ii. The basalts of subgroup 3i lack Th positive anomalies (Th/La_{NMN} = 0.5-0.8), which on the other hand are evident in subgroup 3ii (Th/La_{NMN} = 2.7-4.4). Consequently, the extent of the subduction component seems greater in subgroup 3ii (Th/Nb_{NMN} = 11.0-13.5) than in 3i (Th/Nb_{NMN} = 4.3-4.6). The trace element concentrations of Group 3 basalts largely encompass the compositions of the LREE-depleted LOTI basalts from the Los Ranchos Fm. (Escuder-Viruete et al., 2006) (Fig. 5f).

Chemostratigraphic correlation of these volcanic Groups is broadly hindered by extreme shearing, especially in the Ozama shear zone. Nevertheless, intercepts between fault zones in drill holes (e.g., DDH CM-390 at 565-350 meters below surface) indicate that Group 1 underlies both Groups 2 and 3.

4.1.2.2 Andesites

The least altered sample of andesite (with LOI = 3.3 wt. % and very weak signs of silicification and chloritization, Fig. 2) has a SiO_2 content of 61.48 wt. %, Mg# = 54 and low concentration of Na_2O = 0.63 wt. %. In CN REE diagrams (Fig. 6a), the andesites are depleted in LREE relative to MREE (La/Sm_{CN} = 0.6-0.7) and HREE (La/Yb_{CN} = 0.7) and present flat MREE and HREE segments (Sm/Yb_{CN} = 1.0-1.1). Trace element abundances in andesites are similar to those of N-MORB, except for positive Th (Th/La_{NMN} = 2.4-3.8) and negative Nb (Nb/La_{NMN} = 0.2-0.4) and Ti anomalies (Fig. 6b). The extent of subduction component in these rocks is high (Th/Nb_{NMN} =10.1-10.4). The trace element compositions of andesites from the Maimón Fm. overlap with those of felsic volcanic rocks from the Los Ranchos Fm. (Escuder-Viruete et al., 2006) (Fig. 6b).

4.1.2.3 Plagiorhyolites

Least altered plagiorhyolites have SiO_2 contents that range between 73 and 75 wt.%, Mg# between 24 and 40 and relatively high alkali contents (Na_2O = 4.67-5.26 wt. %; K_2O = 1.32-1.40 wt. %). In terms of trace elements (Fig. 6a, b), two plagiorhyolite samples encompass the compositions of andesites but have more pronounced Ti negative anomalies. In contrast, two other plagiorhyolites are markedly depleted in most trace elements and present near flat REE normalized patterns (La/Sm_{CN} = 0.8, Sm/Yb_{CN} = 0.8), negative Eu and moderate Nb (Nb/La_{NMN} = 0.5-1.1) and Th (Th/La_{NMN} =2.9-3.4) anomalies.

4.2. Radiogenic isotope compositions

Figure 7 displays the age-corrected (125 Ma, i.e., the age of first-arc magmas in the Hispaniola segment of the Caribbean island arc, as discussed in Section 5.4; cf. Escuder-Viruete et al., 2014; Torró et al., *accepted*) Nd, Sr and Pb radiogenic isotope compositions of whole-rocks of the studied samples (Table 2). Most of the samples of Groups 1 and 3 have homogeneous Nd radiogenic isotope ratios (0.51282-0.51293) and plot between the compositions of the depleted MORB mantle (DMM) and enriched mantle 2 (EM2) reservoirs (Fig. 7a). Two samples, one of Group 1 and one of Group 3, have significantly lower Nd isotopic ratios (0.51259-0.51263) and are

more proximal to the EM1 composition (Fig. 7a). Group 2 has variable initial $^{143}Nd/^{144}Nd$ (0.51270-0.51298) (Table 2) indicative of a heterogeneous mantle source. Andesites and plagiorhyolites overlap with Groups 1 and 3 in terms of Nd isotopes (Fig. 7a).

Initial Sr radiogenic isotope ratios are similar among the groups of the Maimón meta-volcanic rocks ($0.70383 \leq {}^{87}Sr/^{86}Sr_{(125\ Ma)} \leq 0.70678$) (Fig. 7a). The important alteration experienced by these rocks supports that their bulk Sr isotopic data most probably do not reflect the primary isotopic compositions of the lavas. Relatively high radiogenic $^{87}Sr/^{86}Sr$ ratios decoupled from $^{143}Nd/^{144}Nd$ decrease are commonly ascribed to seawater alteration. Seawater contamination is particularly evident in several samples of Group 1 and one plagiorhyolite which have initial $^{87}Sr/^{86}Sr > 0.70540$ and relatively high $^{143}Nd/^{144}Nd$ (> 0.51280) (Fig, 7a). Alteration most likely induced the very high whole-rock Rb/Sr of one sample of Group 2 (CM 2-2), which leads to overestimate the time-integrated Rb decay since crystallization; for this reason the composition of this samples is not plotted in Fig. 7a. In terms of Nd-Sr radiogenic isotopes, the samples of the Maimón Fm. generally overlap with the IAT igneous suite of the Caribbean, especially with lavas relatively rich in radiogenic Sr (Fig. 7a).

The Maimón metavolcanic rocks normally present Pb isotopic compositions close to the DMM or intermediate between the DMM and EM1 reservoirs (Fig. 7b, c). Except two samples with anomalously radiogenic Pb isotopic ratios likely affected by shallow crustal contamination (e.g., $^{207}Pb/^{204}Pb_{(125\ Ma)}$ = 15.60-15.98; $^{208}Pb/^{204}Pb_{(125\ Ma)}$ = 38.58-38.93), Group 1 generally has homogeneous $^{207}Pb/^{204}Pb_{(125\ Ma)}$ (15.51-15.53) and $^{208}Pb/^{204}Pb_{(125\ Ma)}$ (37.90-37.99) (Fig, 7b, c). On the other hand, the two analysed samples of Group 2 have relatively homogeneous $^{206}Pb/^{204}Pb_{(125\ Ma)}$ (18.22-18.29), and more variable $^{207}Pb/^{204}Pb_{(125\ Ma)}$ (15.51-15.66) and $^{208}Pb/^{204}Pb_{(125\ Ma)}$ (37.95-38.31) than Group 1. Group 3 has $^{207}Pb/^{204}Pb_{(125\ Ma)}$ and $^{208}Pb/^{204}Pb_{(125\ Ma)}$ similar to Group 1 but lower $^{206}Pb/^{204}Pb_{(125\ Ma)}$ (18.08-18.17). Andesites and plagiorhyolites have Pb isotopic compositions that coincide with those of Groups 1 and 3 (Fig, 7b, c). This resemblance supports that felsic lavas (i.e., plagiorhyolites) in the Maimón Fm. formed by crustal anatexis of mafic rocks at the base of the thickened arc crust, similar to SiO_2-rich lavas in the Los Ranchos Fm. (Escuder-Viruete et al., 2006) and Virgin islands (Jolly et al., 2008). In terms of Pb isotopic ratios, the rocks of the Maimón Fm. are commonly less radiogenic than basalts and diorites of the Los Ranchos Fm. and IAT lavas from the Caribbean (Fig. 7b, c).

5. Discussion

5.1. Mantle source, subduction imprint and extent of melt extraction

In island arc settings, absolute abundances and ratios of HFSE (e.g., Nb, Ta) and HREE (e.g., Yb, Lu) measured in basaltic rocks are widely used to assess the enrichment/depletion of the mantle wedge source and to estimate its degree of melting (e.g., Haase et al., 2002; Marchesi et al., 2007; Neill et al., 2013; Pearce and Peate, 1995). On the other hand, ratios involving Th (i.e., Th/Yb, Th/La, Th/Nb) are useful to trace the slab additions to the mantle wedge, due to the common remobilization of this element from subducted sediments (Pearce, 2014, and references therein). At moderate to high degrees of melting in the absence of garnet (as proposed below for this study case), Nb/Yb variations are normally indicative of the relative depletion of the mantle source (Pearce, 1983; Pearce et al., 2005). Increasing metasomatism of the suprasubduction mantle by fluids and melts expelled from the downgoing slab results in increasing Th/Yb (and Th/Nb) in the derived lavas (Pearce and Peate, 1995). Figure 8 shows the Nb/Yb vs Th/Yb systematics of basaltic rocks from the Maimón Fm. The mantle sources of these basalts have Nb/Yb that mostly span from the values of the DMM to that of the depleted DMM (D-DMM) (Workman and Hart, 2005). Nb/Yb of the Maimón basalts are normally lower than those of basalts of the Los Ranchos Fm. (Escuder-Viruete et al., 2006) (Fig. 8), indicating that they are likely to be derived from more depleted mantle sources. All the studied Maimón basaltic rocks depart from the trends of MORB and FAB due to their higher Th/Yb at a given Nb/Yb, and they point to compositions typical of oceanic arc basalts (Pearce, 2014). Group 3 displays a marked bimodal composition: the rocks of the subgroup 3ii have higher Nb/Yb and Th/Yb than those of the subgroup 3i (Fig. 8). On the other hand, Group 1 has lower Th/Yb than Group 3ii and similar variable Nb/Yb (Fig. 8). The two analysed boninitic samples of Group 2 show uneven Th/Yb and Nb/Yb, a variability also seen in terms of Nd-Pb isotopes (Table 2; Fig. 7). The Th/Yb and Nb/Yb bimodality of Groups 2 and 3 may reflect considerable variations in the depletion of the mantle source and slab input, or local contamination by slab melt capable of remobilize both Nb and Th (e.g., Kessel et al., 2005), as proposed for the source of the Los Ranchos boninites (Escuder-Viruete et al., 2006) and some island arc tholeiites from Cuba (Marchesi et al., 2007).

To constrain the geochemical imprint of slab addition and the extent of melt extraction in the mantle sources of the Maimón volcanic rocks, we have compared their variations of Yb_{CN} versus Sm_{CN} with those of melts produced by anhydrous and hydrous fractional melting in the spinel peridotite field (Fig. 9). Modelled melting sources are DMM, D-DMM and the residue of 5% melt extraction from DMM in the garnet peridotite field. Hydrous melting was simulated according to Bizimis et al. (2000) by a stepwise addition of 0.03 wt.% fluid to the melting source before each 0.1% melt increment, to match minimum ~ 5 wt.% fluid at 15% melt extraction in the source of average island arc basalts (Ayers, 1998). The absence of MREE/HREE fractionation in the Maimón

volcanic rocks (Fig. 5), which is normally ascribed to initial melting in the garnet peridotite field (Fig. 9), constrains the depth of melting to < 85 km (Walter, 2003). Figure 9 shows that anhydrous mantle melting in the spinel peridotite field, similar to melting at mid-ocean ridges, does not explain the MREE-HREE variations of the Maimón volcanic rocks. On the other hand, these melt compositions are compatible with increasing addition of different slab fluids to a depleted mantle wedge source similar to DMM or D-DMM, which experienced increasing melt extraction and fluid addition from Group 3 (~ 5-15% melt extraction, 1.5-4.5 wt.% of fluid in the source) to Group 1 (~ 10-18% melt extraction, 3-5.5 wt.% of fluid in the source) and Group 2 (~ 15-20% melt extraction, 4.5-6 wt.% of fluid in the source) (Fig. 9). As field observations support that Group 1 comprises the oldest rocks of the Maimón Fm. (see section 4.1.2.1), these samples likely record the transitional stages of the magmatic activity from initial (MORB-like) FAB to a more mature stage of island arc volcanism. Focused flux of fluids in the mantle wedge might have caused local melting at higher degrees of melt extraction, producing the depleted boninitic lavas of Group 2. Group 3 possibly represents the products of volcanism transitional to stable subduction conditions, when normal IAT are produced at lower melting degrees (e.g., Ishizuka et al., 2014). Higher Sm at a given Yb content in some samples may reflect compositional variations of the fluid issued from the slab (Fig. 9) or contamination by slab melt instead of fluid.

5.2. Contamination of the mantle source by fluids from subducted Atlantic sediments

Insights into the nature and provenance of the slab component can be obtained from variations of the Nd-Pb radiogenic isotopes, which are customarily used in petrogenetic studies of arc volcanic rocks as they are sensitive tracers of slab additions (e.g., Haase et al., 2002; Moghadam et al., 2014; Pearce et al., 2014; Ribeiro et al., 2013). The Maimón Fm. is part of the so-called IAT volcanic suite of the Caribbean, which records the incipient to mature stages of SW-dipping subduction of the Proto-Caribbean (Atlantic) lithosphere beneath the Greater Antilles island arc in the early Cretaceous (e.g., Boschman et al., 2014; Escuder-Viruete et al., 2014; Pindell et al., 2012). Taking into account this paleogeographic configuration, Atlantic pelagic sediments of Cretaceous age (Jolly et al., 2006) are likely sources of crustal material entering the Greater Antilles subduction zone (e.g., Jolly et al., 2008; Marchesi et al., 2007). On the other hand, a depleted mantle source similar to DMM well approximates the starting composition of the mantle wedge prior to slab addition in the case of the Maimón Fm. (Fig. 8). Figure 10 displays mixing models between the isotopic compositions of DMM and those of fluids liberated from Atlantic Cretaceous pelagic sediments (AKPS; Jolly et al., 2006). The Nd isotopic variation of the Maimón volcanic rocks supports that their depleted mantle wedge source was contaminated by up to 2% of fluids liberated from AKPS sediments (Fig. 10a). On the other hand, the Pb isotopic compositions of these rocks, excluding

samples likely influenced by shallow crustal contamination, are consistent with mixing of the pre-subduction mantle with smaller percentages (< 0.2%) of fluids extracted from marine sediments (Fig. 10b, c). This discrepancy in the extent of slab fluid addition to the mantle wedge, especially compared to the higher values obtained by melting models (Fig. 9), suggests that slab fluids derived not only from subducted sediments but also from oceanic igneous crust, which in particular supplied relatively unradiogenic Pb. Similar to other formations of the Caribbean IAT suite (Escuder-Viruete et al., 2006; Jolly et al., 2008; Marchesi et al., 2007), radiogenic isotopes show that the Maimón volcanic rocks generated by contamination of a depleted mantle wedge by fluids extracted from the subducting Proto-Caribbean oceanic crust capped by Atlantic marine sediments. However, the less radiogenic Pb isotope compositions of the Maimón Fm. compared to other IAT suites, including the Los Ranchos Fm. (Fig. 7b, c), support that the meta-volcanic rocks of the Maimón Fm. record more incipient stages of subduction at shallower depths, at which fluids from the slab were mostly liberated from the subducted igneous crust instead of sediments (Schmidt and Poli, 2003).

5.3. The Maimón Formation and the "subduction-initiation rule"

Tectonomagmatic processes connected to subduction initiation imprint diagnostic chemostratigraphic characteristics to proto- and first-arc magmas. Whattam and Stern (2011) encompassed these characteristics in their "subduction-initiation rule", an inventory of lithogeochemical features that subduction-initiation ophiolites should contain. During subduction inception, vertical foundering into the mantle asthenosphere and trench rollback of the subducting plate initially produce MOR-like basalts (namely forearc basalts, FAB; Reagan et al., 2010). If subduction is not aborted at this stage, MOR-like magmatism is succeeded by arc-like magmas (volcanic arc basalts ± boninites; Ishizuka et al., 2011, 2014) erupted synchronously to arc front stabilization and slab-parallel subduction. The shift from MORB- to arc-like magmas would respond to the shift from decompression to flux melting of a progressively more depleted supra-subduction zone (SSZ) mantle source. As subduction progresses, the increasing input of fluids expelled by the downgoing oceanic igneous crust and sediments into the SSZ mantle source triggers fractionation of subduction-sensitive elements, and LILE and Th enrichment in magmas (Ribeiro et al., 2013, 2015; Whattam and Stern, 2011). Although mostly based on recent data from *in situ* dredged and drilled basalts from the IBM forearc (Ishizuka et al., 2011, 2014; Pearce et al, 2015; Reagan et al., 2010; Ribeiro et al., 2013, 2015), the "subduction initiation rule" has proved to be valid for most Tethyan ophiolites (Whattam and Stern, 2011).

LREE-depleted LOTI (Group 1), boninitic (Group 2), and normal LOTI (Group 3) volcanic rocks from the Maimón Fm. display variable negative Nb and positive Th anomalies (Fig. 5) attesting to different degrees of subduction imprint by slab-derived components. Indeed, progressive changes are observed among the different Groups not only in their concentrations of HFSE (Nb, Ta, Zr, Th), but also in REE, LILE (possibly influenced also by sub-solidus mobility) and transitional metals (e.g., Ti and V) (Fig. 11).

From Group 1 (i.e., the oldest rocks according to stratigraphic relationships) to Group 2, the Maimón basalts register depletion in Y and Lu (i.e., HREE), Zr and TiO_2 that suggests general mantle source depletion and/or increasing degrees of melting (Fig. 9). The progressive enrichment in LREE relative to MREE (i.e., higher La/Sm_{CN}) marks the progressive shift from N-MORB-like to flat (island arc tholeiitic) REE patterns. Similar trends are broadly followed from LREE-depleted LOTI basalts to boninites of the Los Ranchos Fm. (Escuder-Viruete et al., 2006) and from FAB to boninites of the IBM forearc (Ishizuka et al., 2011; Reagan et al., 2010) (Fig. 11). Opposed trends (i.e., HREE, Zr and TiO_2 enrichment) from Groups 1 and 2 to Group 3 Maimón volcanic rocks and from boninitic to IAT Los Ranchos basalts (Fig. 11) probably indicate more fertile mantle sources and/or less intense melting (Fig. 9). The decrease of Nb/La_{NMN} ratios from Group 1 to Group 2 (i.e., the Nb anomaly is more conspicuous in the latter) mirrors that from FAB to boninites of the IBM (Fig. 11). Th/Nb_{NMN} (as a proxy of the extent of subduction component) increases from Groups 1 and 2 to Group 3 Maimón basalts, comparable to basalts of the Los Ranchos Fm. and IBM forearc (Fig. 11). Therefore, the progressive changes in geochemical proxies of subduction imprint, mantle melting and source depletion recorded in the Maimón volcanic rocks are generally on a par with trends recognized in subduction-initiation ophiolites (compilation in Whattam and Stern, 2011).

Group 1 Maimón basalts (i.e., LREE-depleted LOTI) display N-MORB-like normalized REE patterns similar to those of FAB from the IBM forearc but have lower REE concentrations (Fig. 5a); this suggests a more depleted mantle source (see below) or higher degrees of melting compared to typical FAB from the IBM. Figure 5b evidences as well the similar compositions in terms of trace immobile elements of Group 1 and lavas transitional from FAB to arc basalts in the IBM arc. Most FAB and transitional basalts from the IBM arc present negative Nb and positive Th anomalies, comparable to those of Group 1 basalts of the Maimón Fm. (Figs. 5b and 11). Pearce et al. (2015) attributed these hybrid compositions to a "*relatively diverse variation in degrees of melting and amount of subducted fluids involved in their genesis*" [sic.]. In order to further assess similarities and differences between the Maimón volcanic rocks and proto- and first-arc magmas of the IBM forearc (Ishizuka et al, 2011; Reagan et al., 2010), we have plotted the compositions of these magma-types on the Ti vs V, Zr and La/Sm diagrams (Fig. 12). On the Ti vs V plot (Fig. 12a), most

Maimón basaltic rocks lie within the field of island arc tholeiites (IAT; Ti/V = 10-20) and only a sample of Group 2 clearly plots in the field of boninites (Ti/V < 10). Most FAB, back-arc basin basalts (BABB) and transitional lavas extruded proximal to the trench also plot in the field of IAT, in contrast to higher Ti/V (> 20) of most MORB and slab-distal FAB and BABB (Pearce, 2014). The Maimón basalts thus generally present Ti/V similar to FAB erupted close to the trench and transitional FAB-arc lavas from the IBM arc. A similar trend is shown by Ti/Zr ratios (Fig. 12b). Finally, we note that most volcanic rocks of the Maimón Fm., including boninite-like samples, have low LREE/MREE (Fig. 12c), and only Group 3 basalts (normal LOTI) have La/Sm > 1. FAB and transitional lavas of the IBM arc show similar variations of La/Sm (Figs. 11 and 12c). In conclusion, most of the Maimón basaltic rocks have trace element variations generally similar to proto- and first-arc lavas generated in the initial stages of oceanic subduction.

Th/Yb and Th/Nb_{NMN} (Figs. 8 and 11) of Group 1 Maimón basalts are distinctive from those of normal FAB in the IBM arc (Ishizuka et al., 2011; Reagan et al., 2010), suggesting a higher slab sediment input to the SSZ mantle source (~ 3-5.5 wt. % slab fluid addition, 0.2-2 % of which liberated by AKPS according to modelling in Figs. 9 and 10). This observation precludes an unequivocal identification of Group 1 Maimón rocks with FAB *ss*. The absence of typical MORB/FAB is reported in the lower lavas of the subduction-initiation Troodos ophiolite (cf. Pearce and Robinson, 2010). Actually, the development and preservation of the entire set of geochemical lithotypes linked to subduction initiation in a given ophiolite depend on many petrological and geodynamical parameters related to the subduction setting itself and the mechanisms of obduction. Some of these parameters are the temperature of the subducting crust (cold vs hot subduction), the development vs absence of trench rollback and its rate and extent, and the mode and substrate of ophiolite emplacement (Tethyan vs Cordilleran ophiolite types) (e.g., Leng et al., 2012; Pearce and Robinson, 2010; Pearce et al., 2014; Ribeiro et al., 2015). A possible explanation of the different extents of slab fluids input in Group 1 Maimón basalts compared to IBM FAB is that, in the case of the Greater Antilles paleo-arc, the release of fluids and/or melts from the downgoing slab may have occurred at shallower depths and at faster rates due to hot subduction (Pearce and Robinson, 2010), as discussed below in the framework of the early evolution of the Caribbean island arc.

5.4. Correlations with ophiolitic rocks in Hispaniola and implications for the geodynamic evolution of the Early Cretaceous Greater Antilles island arc

The metamorphosed basalts and basaltic andesites of the Maimón Fm. exhibit elemental and isotopic compositional variations that harmonize with those of proto- to first-arc lavas in subduction-initiation ophiolites. Stratigraphic relationships in the Maimón Fm. point that the

extrusion of LREE-depleted LOTI basalts (Group 1) (similar to transitional FAB-boninite lavas of the IBM arc) was followed by boninitic (Group 2) and "normal" LOTI (Group 3) volcanism during the formation of a forearc lithosphere. Likewise, the basalts and basaltic andesites of the lower basaltic unit of the Los Ranchos Fm. (contiguous, to the NE, of the Maimón Fm., Fig. 1b), are described as LREE-depleted LOTI (Escuder-Viruete et al., 2006; Torró et al., *accepted*); besides, Escuder-Viruete et al. (2006) reported rare boninites, even though its stratigraphic relationship with the LREE-depleted LOTI basalts is not clear. On the other hand, basalts with "normal" IAT signatures are described in the upper basaltic unit of Los Ranchos (Escuder-Viruete et al., 2006), but they are not present in the Maimón Fm. Therefore, as a whole, chemostratigraphic relationships between volcanic rocks in both these adjacent formations trace the expected geochemical variations of magmas extruded in a forearc setting during the evolution of an intra-oceanic subduction system (see section 5.3; Fig. 11).

The petrogenetic relationships between the Maimón and Los Ranchos formations are open to debate (e.g., Escuder-Viruete et al., 2007a; Horan, 1995; Lewis et al., 2002; Torró et al., 2016a). Inasmuch as the upper Los Ranchos Fm. is composed of (1) basalts with "normal" IAT signatures (Fig. 5e), and (2) thick sedimentary volcanogenic and terrestrial, shallow submarine and subaerial deposits that cap the volcanic sequence (Kesler et al., 1991a, 2005a, b; Torró et al., *accepted*), which are not identified in the Maimón Fm., any possible correlation between these formations is restricted to the Los Ranchos lower basaltic and intermediate plagiorhyolite units. In terms of trace elements, the LREE-depleted LOTI basalts of Los Ranchos are more similar to Group 3 than to Group 1 rocks of the Maimón Fm. (Fig. 5), but their Pb isotopic (Fig. 7b, c) and Nb/Yb ratios (Fig. 8) are generally higher, suggesting a stronger subduction imprint and a mantle source slightly more enriched. In addition, the felsic volcanic rocks of the Maimón Fm. are distinctively more depleted in LREE, and some specimens in REE as a whole, compared to similar rocks of the Los Ranchos Fm. (Fig. 6a). These compositional discrepancies may reflect different spatial and/or temporal scenarios for the genesis of both formations during inception of oceanic subduction.

A mantle peridotitic counterpart that would complete an ophiolitic sequence, together with the forearc-apical arc Early Cretaceous volcanic units from Cordillera Central, has never been designated despite the proximity of the Maimón and Los Ranchos formations to the Loma Caribe peridotite body (Fig. 1). The purely tectonic contact between these crustal arc-related units and the peridotite body, along the Hispaniola fault zone (Fig. 1), avoids an unequivocal connection. The Loma Caribe peridotites have been firstly interpreted as a mantle section linked to the oceanic plume source of the Duarte Fm. (Lewis et al., 2002, 2006) or they have been assigned to a back-arc setting (Escuder-Viruete et al., 2008). More recently, however, Marchesi et al. (2016) related the

Loma Caribe peridotites to a supra-subduction zone setting during the inception and early evolution of the Greater Antilles paleo-island arc in the Early Cretaceous. These authors concluded indeed that the Loma Caribe dunites formed by interaction of residual peridotites with two subduction-related magmas, and pointed to the LREE-depleted LOTI and boninitic lavas of the Maimón and Los Ranchos formations as the most likely volcanic products of these melts. The scenario suggested by Marchesi et al. (2016) for the Loma Caribe peridotites hence couples with that proposed here for the adjacent Maimón and Los Ranchos formations and altogether suggests that these units are genetically related.

Absolute dating of the Maimón Fm. has been unsuccessful, despite our and other workers' (J. Escuder-Viruete personal communication) repeated attempts for obtaining U-Pb zircon and Ar-Ar amphibole ages. In the light of its relatively geochemical similitude to volcanic rocks of the lower Los Ranchos Fm., the age of the Maimón Fm. has been commonly bracketed as Barremian - Early Aptian (Escuder-Viruete et al., 2007a; Horan, 1995; Torró et al., 2016a). The intrusion at 125.4 ± 0.4 Ma of gabbroic sills with a weak subduction imprint into the Loma Caribe peridotites (Escuder-Viruete et al., 2010) amply agrees with the timing proposed for the extrusion of the Maimón basalts. This inferred time range is in good agreement with the age of the onset of arc-related magmatism in the Hispaniola segment of the Caribbean island-arc (~ 126 Ma), proposed by Escuder-Viruete et al. (2014) based on the study of plutonic rocks from the Puerto Plata ophiolitic complex in N Hispaniola. The lithogeochemical evolution of basaltic melts in the Puerto Plata ophiolitic complex matches similar variations in Cordillera Central (Escuder-Viruete et al., 2014), with the caveat that in the Maimón and Los Ranchos formations this progression is entirely recorded by volcanic material.

Pindell et al. (2012) proposed that the onset of SW-directed subduction of the Proto-Caribbean lithosphere beneath the Caribbean Plate occurred at ca. 135 Ma in the context of a trench-to-trench 'inter-American' transform fault, which connected the NE-facing arc in the western flank of the Americas (see their Figs. 2 and 3). In this model, the transform fault delineated the contact between the Caribbean (Pacific) and the Proto-Caribbean (Atlantic) oceanic lithospheres, and a trench-trench-ridge triple junction occurred in its contact with the spreading ridge across the Proto-Caribbean lithosphere (Fig. 13a) (see also Boschman et al., 2014). Underthrusting of the young Proto-Caribbean slab would have resulted in a 'hot' subduction scenario in which slab dehydration is favoured and, in end-member cases, it is broadly complete before reaching normal sub-arc depths (e.g., Mullen and McCallum, 2014). This scenario would therefore be consistent with a conspicuous slab fluid addition to the mantle source of the Maimón Fm. (Figs. 8-10) at relatively shallow levels in a forearc position during the generation of transitional proto- to first-arc melts (Fig. 13b-d). On

the other hand, this reconstruction contrasts with intense slab dehydration beneath the arc front expected in cold subduction settings such as the Mariana arc (Ribeiro et al., 2015 and references therein).

Subduction of an oceanic ridge and associated warm, young oceanic lithosphere during the Early and mid-Cretaceous time is recorded in the Sierra del Convento (Garcia-Casco et al., 2008b; Lázaro and García Casco, 2008; Lázaro et al., 2009) and La Corea (Blanco-Quintero et al., 2010, 2011a, b) mélanges in eastern Cuba. In both mélange units, trondhjemitic-tonalitic melts with adakitic signatures generated after partial melting of subducted amphibolites with MORB-affinities in the mantle wedge, indicating a very high thermal gradient connected to the subduction of the Proto-Caribbean. Blanco-Quintero et al. (2010; see Fig. 13 therein) proposed a model with the likely locations of the La Corea and Sierra del Convento (eastern Cuba) and the Río San Juan (Dominican Republic) mélanges relative to the subducting Proto-Caribbean ridge; within this model, we envisage the formation of the volcanic arc segment represented in the Maimón Formation somewhere between the Río San Juan Complex (cf. Escuder-Viruete et al., 2013; Krebs et al., 2011) and the vertical projection of the ridge in the overriding plate. Subsequently, the Late Eocene to present transpressional tectonic regime and related left-lateral strike-slip faults would have driven the NW to SE drift of the Maimón Formation to its current location in the Central belt of the Dominican Cordillera Central.

We finally remark that the mantle sources of the Maimón volcanic rocks were in general more depleted than average DMM (Fig. 8). Oceanic spreading prior to subduction initiation beneath the NE limit of the Caribbean Plate occurred both in the Pacific (Panthalassa ocean, prior that the Caribbean became a separate plate, and then the Caribbean) and Atlantic (Proto-Caribbean) domains, and was due to the break-up of Pangea (Boschman et al., 2014, and references therein). In the proposed scenario of SW-dipping subduction, Atlantic depleted, shallow asthenospheric mantle might have ascended to fill the mantle wedge created by the vertical foundering of the Proto-Caribbean Plate. Moreover, Proto-Caribbean asthenospheric mantle may also have ascended into the wedge by return flow or through the propagation of the subducting Proto-Caribbean mid-ocean ridge (Fig. 13b-c herein; cf. Pearce and Robinson, 2010; Pearce et al., 2014). Mantle melting in these conditions would be responsible for the marked compositional heterogeneity of the Loma Caribe peridotites (Marchesi et al., 2016) and proto- and first-arc basalts of the Maimón and Los Ranchos formations.

6. Conclusions

(1) From the lower to upper units, the metabasaltic rocks of the Early Cretaceous Maimón Fm. (Cordillera Central, Dominican Republic) shift from LREE-depleted low Ti tholeiites (LOTI; Group 1), similar to forearc basalts, to boninite-like lavas (Group 2) and LREE-richer (normal) LOTI (Group 3). These variations mirror the geochemical evolution from proto- to first-arc lavas documented in subduction-initiation ophiolites.

(2) The Maimón parental magmas were generated by hydrous melting of a spinel-facies DMM/D-DMM source fluxed by fluids from subducted oceanic crust and Atlantic Cretaceous pelagic sediments. Group 1 rocks, which record magmatic stages transitional from forearc basalts to boninitic magmas, formed by ~ 10-18 % melt extraction and 3.5 to 5.5 wt. % fluid addition in the source. Group 2 resulted from higher degrees of melt extraction (15-20 %) linked to more intense flux of fluids (4.5-6 wt. % in the source). Group 3 basalts, which probably extruded during transition to the first steady-state subduction-related magmas, formed by ~ 5-15 % melt extraction and 1.5-4.5 wt. % fluid addition.

(3) Nd-Pb isotopic compositions of plagiorhyolites are similar to those of metabasaltic rocks, supporting that they generated by anatexis at the base of the arc crust.

(4) Although both the Maimón and Los Ranchos volcanic formations in the Cordillera Central record magmatic evolutions during subduction-initiation, they probably formed in slightly different spatial/temporal settings within the forearc-arc segment. The recent assignation of the close Loma Caribe peridotites to a subduction-initiation sub-arc mantle setting suggests that these mantle and crustal units are genetically connected.

(5) Our data support the SW-directed subduction of the young and warm Proto-Caribbean lithosphere beneath the Caribbean Plate during the Early Cretaceous. A hot subduction scenario agrees with intense melting and flux of slab fluids in the mantle source of the proto- and first-arc magmas of the Maimón Formation.

Acknowledgements

This research has been funded by the Spanish project CGL2012-36263, the Dominican project 2014-1B4-132, the Catalan project 2014-SGR-1661 and a FPU Ph.D. grant to L.T. by the Ministerio de Educación of the Spanish Government. C.M. acknowledges funding by Ramón y Cajal Fellowship RYC-2012-11314 granted by the Spanish "Ministerio de Economía y Competitividad" (MINECO). The University of Granada partially funded XRF and ICP-MS analyses. The help and hospitality extended by the staff of the Cerro de Maimón mine during

sampling and the logistical support by Perilya-CORMIDOM are also gratefully acknowledged, with special reference to Cevero Chavez, Ricardo del Carpio and Paulo León. We are grateful to Dr. I. Neill and an anonymous reviewer for sound and accurate reviews and to Dr. A.C. Kerr for the competent editorial handling.

References

Ayers, J.C., 1998. Trace element modeling of aqueous fluid–peridotite interaction in the mantle wedge of subduction zones. Contributions to Mineralogy and Petrology 132, 390–404.

Beccaluva, I., Coltori, M., Giunta, G., Siena, F., 2004. Tethyan vs. Cordilleran ophiolites: a reappraisal of distinctive tectonomagmatic features of supra-subduction complexes in relation to the subduction mode. Tectonophysics 393, 163-174.

Bedini, R.M., Bodinier, J.-L., 1999. Distribution of incompatible trace elements between the constituents of spinel peridotite xenoliths: ICP-MS data from the East African Rift. Geochimica et Cosmochimica Acta 63, 3883–3900.

Bizimis, M., Salters, V.J.M., Bonatti, E., 2000. Trace and REE content of clinopyroxenes from supra-subduction zone peridotites. Implications for melting and enrichment processes in island arcs. Chemical Geology 165, 67-85.

Blanco-Quintero, I.F., Garcia-Casco, A., Rojas-Agramonte, Y., Rodríguez-Vega, A., Lázaro, C., Iturralde-Vinent, M.A., 2010. Metamorphic evolution of subducted hot oceanic crust (La Corea Mélange, Cuba). American Journal of Science 310, 889-915.

Blanco-Quinero, I.F., Rojas-Agramonte, Y., García-Casco, A., Kröner, A., Mertz, D.F., Lázaro, C., Blanco-Moreno, J., Renne, P.R., 2011a. Timing of subduction and exhumation in a subduction channel: Evidence from slab melts from La Corea Mélange (eastern Cuba). Lithos 127, 86-100.

Blanco-Quintero, I.F., Gerya, T.V., García-Casco, A., Castro, A., 2011b. Subduction of young oceanic plates: A numerical study with application to aborted thermal-chemical plumes. Geochemistry Geophysics Geosystems 12, Q10012 (DOI: 10.1029/2011gc003717)

Blein, O., Guillot, S., Lapierre, H., Mercier de Lépinay, B., Lardeaux, J.M., Millán Trujillo, G., Campos, M., García, A., 2003. Geochemistry of the Mabujina Complex, central Cuba: implications on the Cuban Cretaceous Arc Rocks. The Journal of Geology 111, 89-101.

Boschman, L.M., van Hinsbergen, D.J.J., Torsvik, T.H., Spakman, W., Pindell, J.L., 2014. Kinematic reconstruction of the Caribbean region since the Early Jurassic. Earth-Science Reviews 138, 102-136.

Bowin, C.O., 1966. Geology of the central Dominican Republic. Geological Society of America Memoirs 98, 11-84.

Chernyshev, I.V., Chugaev, A.V., Shatagin, K.N., 2007. High-precision Pb isotope analysis by multicollector-ICP-mass-spectrometry using $^{205}Tl/^{203}Tl$ normalization: optimization and calibration of the method for the studies of Pb isotope variations. Geochemistry International 45, 1065-1076.

Cumming, G.L., Kesler, S.E., 1987. Lead isotopic composition of the oldest volcanic rocks of the Eastern Greater Antilles island arc. Chemical Geology 65, 15-23.

Dilek, Y., Furnes, H., 2014. Ophiolites and their origins. Elements 10, 93-100.

Donnelly, K.E., Goldstein, S.L., Langmuir, C.H., Spiegelman, M., 2004. Origin of enrichedocean ridge basalts and implications for mantle dynamics. Earth and Planetary Science Letters 226, 347–366.

Draper, G. and Gutiérrez-Alonso, G., 1997. La estructura del cinturón de Maimón en la Isla de Hispaniola y sus implicaciones geodinámicas. Revista de la Sociedad Geológica de España 10, 281-299.

Draper, G., Gutiérrez, G., Lewis, J.F., 1996. Thrust emplacement of the Hispaniola peridotite belt: orogenic expression of the mid Cretaceous Caribbean arc polarity reversal? Geology 24, 1143-1146.

Escuder-Viruete, J., Díaz de Neira, A., Hernáiz Huerta, P.P., Monthel, J., García Senz, J., Joubert, M., Lopera, E., Ullrich, T., Friedman, R., Mortensen, J., Pérez-Estaún, A., 2006. Magmatic relationships and ages of Caribbean island-arc tholeiites, boninites and related felsic rocks, Dominican Republic. Lithos 90, 161-186.

Escuder-Viruete, J., Contreras, F., Joubert, M., Urien, P., Stein, G., Weis, D., Pérez-Estaún, A., 2007a. Tectónica y geoquímica de la Formación Amina: registro del arco isla Caribeño primitivo en la Cordillera Central, República Dominicana. Boletín Geológico y Minero 118, 221-242.

Escuder-Viruete, J., Perez-Estaún, A., Contreras, F., Joubert, M., Weis, D., Ullrich, T., Spades, P., 2007b. Plume mantle source heterogeneity through time: Insights from the Duarte complex, Hispaniola, northeastern Caribbean. Journal of Geophysical Research 112, B04203.

Escuder-Viruete, J., Contreras, F., Stein, G., Urien, P., Joubert, M., Pérez-Estaún, A., Friedman, R., Ullrich, T., 2007c. Magmatic relationships between adakites, magnesian andesites and Nb-enriched basalt-andesites from Hispaniola: Record of a major change in the Caribbean island arc magma sources. Lithos 99, 151-177.

Escuder-Viruete, J., Joubert, M., Urien, P., Friedman, R., Weis, D., Ullrich, T., Pérez-Estaún, A., 2008. Caribbean island-arc rifting and back-arc basin development in the Late Cretaceous: Geochemical, isotopic and geochronological evidence from Central Hispaniola. Lithos 104, 378-404.

Escuder-Viruete, J., Pérez-Estaún, A., Weis, D., 2009. Geochemical constraints on the origin of the late Jurassic proto-Caribbean oceanic crust in Hispaniola. International Journal of Earth Sciences 98, 407-425.

Escuder-Viruete, J., Pérez-Estaún, A., Weis, D., Friedman, R., 2010. Geochemical characteristics of the Río Verde Complex, Central Hispaniola: Implications for the paleotectonic reconstruction of the Lower Cretaceous Caribbean island-arc. Lithos 114, 168-185.

Escuder-Viruete, J., Perez-Estaun, A., Joubert, M., Weis, D., 2011. The Pelona-Pico Duarte basalts formation, Central Hispaniola: An on-land section of Late Cretaceous volcanism related to the Caribbean large igneous province. Geologica Acta 9, 307-328.

Escuder-Viruete, J., Valverde-Vaquero, P., Rojas-Agramonte, Y., Gabites, J., Castillo-Carrión, M., Pérez-Estaún, A., 2013. Timing of deformational events in Río San Juan complex: Implications for the tectonic controls on the exhumation of high-P rocks in the northern Caribbean subduction-accretionary prism. Lithos 177, 416-435.

Escuder-Viruete, J., Castillo-Carrión, M., Pérez-Estaún, A., 2014. Magmatic relationships between depleted mantle harzburgites, boninitic cumulate gabbros and subduction-related tholeiitic basalts in the Puerto Plata ophiolitic complex, Dominican Republic: Implications for the birth of the Caribbean Island-arc. Lithos 196-197, 261-280.

Escuder-Viruete, J., Joubert, M., Abad, M., Pérez-Valera, F., Gabites, J., 2016. The basaltic volcanism of the Dumisseau Formation in the Sierra de Bahoruco, SW Dominican Republic:

A record of the mantle plume-related magmatism of the Caribbean Large Igneous Province. Lithos 254-255, 67-83.

Gaetani, G.A., Kent, A.J.R., Grove, T.L., Hutcheon, I.D., Stolper, E.M., 2003. Mineral/melt partitioning of trace elements during hydrous peridotite partial melting. Contributions to Mineralogy and Petrology 145, 391–405.

Garcia-Casco, A., Iturralde-Vinent, M.A., Pindell, J., 2008a. Latest Cretaceous collision/accretion between the Caribbean plate and Caribeana: origin of metamorphic terranes in the Greater Antilles. International Geology Review 50, 781-809.

Garcia-Casco, A., Lázaro, C., Rojas-Agramonte, Y., Kröner, A., Torres-Roldán, R.L., Núñez, K., Neubauer, F., Millán, G., Blanco-Quinero, I., 2008b. Partial Melting and Counterclockwise P-T Path of Subducted Oceanic Crust (Sierra del Convento Mélange, Cuba). Journal of Petrology 49, 129-161.

Govindaraju, K., 1994. Compilation of working values and sample description for 383 geostandards. Geostandards and Geoanalytical Research 18, 1-158.

Govindaraju, K., Potts, P.J., Webb, P.C., Watson J.S., 1994. Report on Whin Sill Dolerite WS-E from England and Pitscurrie Micrograbbro PM-S from Scotland: Assessment by one hundred and four international laboratories. Geostandards Newsletters 18, 211-300.

Haase, K.M., Worthington, T.J., Stoffers, P., Garbe-Schönberg, D., Wright, I., 2002. Mantle dynamics, element recycling, and magma genesis beneath the Kermadec Arc-Havre Trough. Geochemistry Geophysics Geosystems 3, 1071. DOI: 10.1029/2002GC000335.

Hastie, A.R., Kerr, A.C., Pearce, J.A., Mitchell, S.F., 2007. Classification of altered island arc rocks using immobile trace elements: development of the Th-Co discrimination diagram. Journal of Petrology 48, 2341-2357.

Hofmann, A.W., 2003. Sampling mantle heterogeneities through oceanic basalts: isotopes and trace elements, in: Carlson, R.W. (Ed.), Treatise on Geochemistry, The Mantle and the Core, Vol. 2. Elsevier, Amsterdam, pp. 61-101.

Hollis, S.P., Roberts, S., Earls, G., Herrington, R., Cooper, M.R., Piercey, S.J., Archibald, S.M., Moloney, M., 2014. Petrochemistry and hydrothermal alteration within the Tyrone Igneous Complex, Northern Ireland: implications for VMS mineralization in the British and Irish Caledonides. Mineralium Deposita 49, 575-593.

Horan, S.L., 1995. The geochemistry and tectonic significance of the Maimón-Amina schists, Cordillera Central, Dominican Republic. Unpublished M.S. thesis, University of Florida, Gainesville.

Irvine, T.N. Baragar, W.R., 1971. A guide to the chemical classification of the common igneous rocks. Canadian Journal of Earth Sciences 8, 523-548.

Ishizuka, O., Tani, K., Reagan, M.K., Kanayama, K., Umino, S., Harigane, Y., Sakamoto, I., Miyajima, Y., Yuasa, M., and Dunkley, D.J., 2011. The timescales of subduction initiation and subsequent evolution of an oceanic island arc. Earth and Planetary Science Letters 306, 229-240.

Ishizuka, O., Tani, K., Reagan, M.K., 2014. Izu-Bonin-Mariana Forearc Crust as a Modern Ophiolite Analogue. Elements 10, 115-120.

Jensen, L.S., 1976. A new cation plot for classifying subalkalic volcanic rocks. Miscellaneous Paper, 66, Ontario Department of Mines, Canada.

Johnson, M.C., Plank, T., 1999. Dehydration and melting experiments constrain the fate of subducted sediments. Geochemistry, Geophysics, Geosystems 1, DOI 10.1029/1999GC000014

Johnson, K.T.M., Dick, H.J.B., Shimizu, N., 1990. Melting in the oceanic upper mantle: an ion microprobe study of diopsides in abyssal peridotites. Journal of Geophysical Research 95, 2661–2678.

Jolly, W.T., Lidiak, E.G., Dickin, A.P., 2006. Cretaceous to Mid-Eocene pelagic sediment budget in Puerto Rico and the Virgin Islands (northeast Antilles Island Arc). Geologica Acta 4, 35-62.

Jolly, W. T., Lidiak, E. G., and Dickin, A. P., 2008. The case for persistent southwest-dipping Cretaceous convergence in the northeast Antilles: Geochemistry, melting models, and tectonic implications. Geological Society of America Bulletin 20, 1036-1052.

Kerr, A.C., White, R.V., Thompson, P.M.E., Tarney, J., Saunders, A.D., 2003. No oceanic plateau-No Caribbean Plate? The seminal role of an oceanic plateau in Caribbean Plate evolution, in: Bartolini, C., Buffler, R.T., Blickwede, J.F. (Eds.), The Circum-Gulf of Mexico and Caribbean Region: Hydrocarbon habitats, basin formation and plate Tectonics. American Association of Petroleum Geologists Memoir, 79, AAPG, Tulsa, pp. 126-168.

Kesler, S.E., Russell, N., Polanco, J., McCurdy, K., Cumming, G.L., 1991a. Geology and geochemistry of the early Cretaceous Los Ranchos Formation, central Dominican Republic, in: Mann, P., Draper, G., Lewis, J.F. (Eds.), Geologic and tectonic development of the North American: Caribbean plate boundary in Hispaniola. Geological Society of America Special Papers 262, 187-201.

Kesler, S., Russell, E.N., Reyes, C., Santos, L., Rodriguez, A., Fondeur, L., 1991b. Geology of the Maimon Formation, Dominican Republic, in: Mann, P., Draper, G., Lewis, J.F. (Eds.), Geologic and tectonic development of the North American: Caribbean plate boundary in Hispaniola. Geological Society of America Special Papers 262, 173-185.

Kesler, S.E., Campbell, I.H., Allen, C.M., 2005a. Age of the Los Ranchos Formation, Dominican Republic: Timing and tectonic setting of primitive island arc volcanism in the Caribbean region. Geological Society of America Bulletin 117, 987-995.

Kesler, S.E., Campbell, I.H., Smith, C.N., Hall, C.M., Allen, C.M., 2005b. Age of the Pueblo Viejo Gold-Silver Deposits and Its Significance to Models for High-Sulfidation Epithermal Mineralization. Economic Geology 100, 253-272.

Kessel, R., Schmidt, M., Ulmer, P., Pettke, T., 2005. Trace element signature of subduction-zone fluids, melts and supercritical liquids at 120-180 km depth. Nature 437, 724-727.

Krebs, M., Schertl, H.P., Maresch, W.V., Draper, G., 2011. Mass flow in serpentinite-hosted subduction channels: P–T–t path patterns of metamorphic blocks in the Rio San Juan mélange (Dominican Republic). Journal of Asian Earth Sciences 42, 569-595.

Lázaro, C., García-Casco, A., 2008. Geochemical and Sr-Nd isotope signatures of pristine slab melts and their residues (Sierra del Convento mélange, eastern Cuba). Chemical Geology 255, 120-133.

Lázaro, C., García-Casco, A., Rojas-Agramonte, Y., Kröner, A., Neubauer, F., Iturralde-Vinent, M., 2009. Fifty-five-million-year history of oceanic subduction and exhumation at the northern edge of the Caribbean plate (Sierra del Convento mélange, Cuba). Journal of Metamorphic Geology 27, 19-40.

Lázaro, C., Blanco-Quintero, I.F., Proenza, J.A., Rojas-Agramonte, Y., Neubauer, F., Núñez-Cambra, K., García-Casco, A., 2016. Petrogenesis and 40Ar/39Ar dating of proto-forearc

crust in the Early Cretaceous Caribbean arc: The La Tinta mélange (eastern Cuba) and its easterly correlation in Hispaniola. International Geology Review 58, 1020-1040.

Leng, W., Gurnis, M., Asimow, P., 2012. From basalts to boninites: The geodynamics of volcanic expression during induced subduction initiation. Lithosphere 4, 511-523.

Lewis, J.F. Draper, G., 1990. Geology and tectonic evolution of the Northern Caribbean margin, in: Dengo, G., Case, J.E. (Eds.), The Caribbean region. Geological Society of America, The Geology of North America, H, Boulder, pp. 77-140.

Lewis, J.F., Amarante, A., Bloise, G., Jiménez, J.G., Dominguez, H.D., 1991. Lithology and stratigraphy of upper Cretaceous volcanic and volcaniclastic rocks of the Tireo Group, Dominican Republic, and correlations with the Massif du Nord in Haiti, in: Mann, P., Draper, G., Lewis, J.F. (Eds.), Geologic and tectonic development of the North American: Caribbean plate boundary in Hispaniola. Geological Society of America Special Papers 262, 143-164.

Lewis, J.F., Astacio, V.A., Espaillat, J., Jiménez, J., 2000. The occurrence of volcanogenic massive sulfide deposits in the Maimón Formation, Dominican Republic: The Cerro de Maimón, Loma Pesada and Loma Barbuito deposits, in: Sherlock, R., Barsch, R., Logan, A. (Eds.), VMS deposits of Latin America. Geological Society of Canada Special Publication 2, 213-239.

Lewis, J.F., Escuder Viruete, J., Hernaiz Huerta, P.P., Gutiérrez, G., Draper, G., 2002. Subdivisión geoquímica del arco de isla Circum-Caribeño, Cordillera Central Dominicana: implicaciones para la formación, acreción y crecimiento cortical en un ambiente intraoceánico. Acta Geologica Hispanica 37, 81-122.

Lewis, J.F., Draper, G., Proenza, J.A., Espaillat, J., Jiménez, J., 2006. Ophiolite-Related Ultramafic Rocks (Serpentinites) in the Caribbean Region: A Review of the Occurrence, Composition, Origin, Emplacement and Ni-Laterite Soil Formation. Geologica Acta 4, 237-263.

Lidiak, E.G., Anderson, T.H., 2015. Evolution of the Caribbean plate and origin of the Gulf of Mexico in light of plate motions accommodated by strike-slip faulting, in: Anderson, T.H., Didenko, A.N., Johnson, C.L., Khanchuk, A.I., MacDonald, J.H., Jr. (Eds.), Late Jurassic Margin of Laurasia—A Record of Faulting Accommodating Plate Rotation: Geological Society of America Special Paper 513, SPE513–01.

Lidiak, E.G., Jolly, W.T., Dickin, A.P., 2011. Pre-arc basement complex and overlying early island arc strata, Southwestern Puerto Rico: overview, geologic evolution and revised data bases. Geologica Acta 9, 273-287.

Maffione, M., Thieulot, C., van Hinsbergen, D.J.J., Morris, A., Plümper, O., Spakman, W., 2015. Dynamics of intra-oceanic subduction initiation: 1: Oceanic detachment fault inversion and the formation of supra-subduction zone ophiolites. Geochemistry Geophysics Geosystems 16, 1753-1770.

Mann, P., Draper, G., Lewis, J.F., 1991. An overview of the geologic and tectonic development of Española, in: Mann, P., Draper, G., Lewis, J.F. (Eds.), Geologic and tectonic development of the North American: Caribbean plate boundary in Hispaniola. Geological Society of America Special Papers 262, 1-28.

Mann, P., Calais, E., Ruegg, J.C., DeMets, C., Jansma, P.E., Mattioli, G.S., 2002. Oblique collision in the northeastern Caribbean from GPS measurements and geological observations. Tectonics 21, 1057.

Marchesi, C., Garrido, C.J., Godard, M., Proenza, J.A., Gervilla, F., Blanco-Moreno, J., 2006. Petrogenesis of highly depleted peridotites and gabbroic rocks from the Mayarí-Baracoa Ophiolitic Belt (eastern Cuba). Contributions to Mineralogy and Petrology 151, 717-736.

Marchesi, C., Garrido, C.J., Bosch, D., Proenza, J.A., Gervilla, F., Monié, P., Rodríguez-Vega, A., 2007. Geochemistry of Cretaceous Magmatism in Eastern Cuba: Recycling of North American Continental Sediments and Implications for Subduction Polarity in the Greater Antilles. Journal of Petrology 48, 1813-1840.

Marchesi, C., Jolly, W.T., Lewis, J.F., Garrido, C.J., Proenza, J.A., Lidiak, E.G., 2011. Petrogenesis of fertile mantle peridotites from the Monte del Estado massif (Southwest Puerto Rico): a preserved section of Proto-Caribbean lithospheric mantle? Geologica Acta 9, 289-306.

Marchesi, C., Garrido, C.J., Proenza, J.A., Hidas, K., Varas-Reus, M.I., Butjosa, L., Lewis, J.F., 2016. Geochemical record of subduction initiation in the sub-arc mantle: Insights from the Loma Caribe peridotite (Dominican Republic). Lithos 252-253, 1-15.

Martín, M., Draper, G., 1999. Mapa geológico de la hoja 6172-I (Hatillo) a escala 1:50 000 (SYSMIN, Proyecto C). Consorcio ITGE-PROINTEC-INYPSA. Dirección General de Minería, Santo Domingo.

Mattinson, J.M., Pessagno, E.A., Montgomery, H., Hopson, C.A., 2008. Late Jurassic age of oceanic basement at La Désirade Island, Lesser Antilles Arc. Geological Society of America Special Papers 438, 175-190.

Mcdonough, W.F., Sun, S.S., 1995. The composition of the Earth. Chemical Geology 120, 223-253.

Meffre, S., Aitchison, J.C., Crawford, A.J., 1996. Geochemical evolution and tectonic significance of boninites and tholeiites from Koh ophiolite, New Caledonia. Tectonics 15, 67-83.

Moghadam, H.S., Khedr, M.Z., Chiaradia, M., Stern, R.J., Bakhshizad, F., Arai, S., Ottley, C.J., Tamura, A., 2014. Supra-subduction zone magmatism of the Neyriz ophiolite, Iran: constraints from geochemistry and Sr-Nd-Pb isotopes. International Geology Review 56, 1395-1412.

Montero, P., Bea, F., 1998. Accurate determination of $^{87}Rb/^{86}Sr$ and $^{147}Sm/^{144}Nd$ ratios by inductively-coupled-plasma mass spectrometry in isotope geoscience: an alternative to isotope dilution analysis. Analytica Chimica Acta 358, 227-233.

Moores, E.M., 1982. Origin and emplacement of ophiolites. Reviews in Geophysics and and Space Physics 20, 735-760.

Mullen, E.K., McCallum, I.S., 2014. Origin of Basalts in a Hot Subduction Setting: Petrological and Geochemical Insights from Mt. Baker, Northern Cascade Arc. Journal of Petrology 55, 241-281.

Myczynski, R., Iturralde-Vinent, M., 2005. The Late Lower Albian invertebrate fauna of the Rio Hatillo Formation of Pueblo Viejo, Dominican Republic. Caribbean Journal of Science 41, 782-796.

Neill, I., Gibbs, J.A., Hastie, A.R., Kerr, A.C., 2010. Origin of the volcanic complexes of La Désirade, Lesser Antilles: Implications for tectonic reconstruction of the Late Jurassic to Cretaceous Pacific-proto Caribbean margin. Lithos 120, 407-420.

Neill, I., Kerr, A.C., Hastie, A.R., Pindell, J.L., Millar, I.L., Atkinson, N., 2012. Age and Petrogenesis of the Lower Cretaceous North Coast Schist of Tobago, a Fragment of the Proto–Greater Antilles Inter-American Arc System. The Journal of Geology 120, 367-384.

Neill, I., Kerr, A.C., Hastie, A.R., Pindell, J.L., Millar, I.L., 2013. The Albian-Turonian Island Arc Rocks of Tobago, West Indies: Geochemistry, Petrogenesis, and Caribbean Plate Tectonics. Journal of Petrology 54, 1607-1639.

Neill, I., Kerr, A.C., Chamberlain, K.R., Schmitt, A.K., Urbani, F., Hastie, A.R., Pindell, J.L., Barry, T.L., Millar, I.L., 2014. Vestiges of the proto-Caribbean seaway: Origin of the San Souci Volcanic Group, Trinidad. Tectonophysics 626, 170-185.

Nelson, C.E., Proenza, J.A., Lewis, J.F., López-Kramer, J., 2011. The metalogenic evolution of the Greater Antilles. Geologica Acta 9, 229-264.

Niu, Y., 1997. Mantle melting and melt extraction processes beneath ocean ridges: evidence from abyssal peridotites. Journal of Petrology 38, 1047–1074.

Pearce, J.A., 1983. The role of sub-continental lithosphere in magma genesis at destructive plate margins, in: Hawkesworth, C.J., Norris, M.J. (Eds.), Continental Basalts and Mantle Xenoliths. Nantwich, Shiva, pp. 230-249.

Pearce, J.A., 1996. A user's guide to basalt discrimination diagrams. Geological Association of Canada Special Publication 12, 79-113.

Pearce, J.A., 2014. Immobile elements fingerprinting of ophiolites. Elements 10, 101-108.

Pearce, J.A., Peate, D.W., 1995. Tectonic implications of the composition of volcanic arc magmas. Annual Review of Earth and Planetary Sciences 23, 251-285.

Pearce, J.A., Robinson, P.T., 2010. The Troodos complex probably formed in a subduction initiation, slab edge setting. Gondwana Research 18, 60-81.

Pearce, J.A., Stern, R.J., Bloomer, S.H., Fryer, P., 2005. Geochemical mapping of the Mariana arc-basin system: Implications for the nature and distribution of subduction components. Geochemistry Geophysics Geosystems 6, Q07006.

Pearce, J.A., Hastie, A.R., Leat, P.T., Dalziel, I.W., Lawver, L.A., Barker, P.F., Millar, I.L. Barry, T.L., Bevins, R.E., 2014. Compositions and evolution of the Ancestral South Sandwich Arc: Implications for the flow of deep ocean water and mantle through the Drake Passage Gateway. Global and Planetary Change 213, 298-322.

Pearce, J.A., Reagan, M.K., and other 26 Expedition 352 Scientists, 2015. Izu-Bonin-Mariana fore arc: Testing subduction initiation and ophiolite models by drilling the outer Izu-Bonin-Mariana fore arc. International Ocean Discovery Program Preliminary Report, 352. http://dx.doi.org/10.14379/iodp.pr.352.2015

Pindell, J.L., Maresch, W.V., Martens, U., Stanek, K.P., 2012. The Greater Antillean Arc: Early Cretaceous origin and proposed relationship to Central American subduction mélanges: Implications for models of Caribbean evolution. International Geology Reviews 54, 131-143.

Proenza, J.A., Zaccarini, F., Lewis, J.F., Longo, F., Garuti, G., 2007. Chromian spinel composition and the platinum-group minerals of the PGE-rich Loma Peguera chromitites, Loma Caribe peridotite, Dominican Republic. Canadian Mineralogist 45, 631-648.

Reagan, M.K., Ishizuka, O., Tsukuaba, H., Stern, R.J., Kelley, K.A., Ohara, Y., Blichert-Toft, J., Bloomer, S.H., Cash, J., Fryer, P., Hanan, B.B., Hickey Vargas, R., Ishii, T., Kimura, J.I., Peate, D.W., Rowe, M.C., Woods, M., 2010. Forearc basalts and subduction initiation in the Izu-Bonin-Mariana system. Geochemistry Geophysics Geosystems 11, DOI: 10.1029/2009GC002871.

Ribeiro, J.M., Stern, R.J., Kelley, K.A., Martinez, F., Ishizuka, O., Manton, W.I., Ohara, Y., 2013. Nature and distribution of slab-derived fluids and mantle sources beneath the Southeast Mariana forearc rift. Geochemistry Geophysics Geosystems 14, 4585-4607.

Ribeiro, J.M., Stern, R.J., Kelley, K.A., Shaw, A.M., Martinez, F., Ohara, Y., 2015. Composition of the slab-derived fluids released beneath the Mariana forearc: Evidence for shallow dehydration of the subducting plate. Earth and Planetary Science Letters 418, 136-148.

Rojas-Agramonte, Y., Kröner, A., Garcia-Casco, A., Somin, M., Iturralde-Vinent, M.A., Mattinson, J.M., Millán Trujillo, G., Sukar, K., Pérez Rodríguez, M., Carrasquilla, S., Wingate, M.T.D., Liu, D.Y., 2011. Timing and Evolution of Cretaceous Island Arc Magmatism in Central Cuba: Implications for the History of Arc System in the Northwestern Caribbean. The Journal of Geology 119, 619-640.

Rojas-Agramonte, Y., Garcia-Casco, A., Kemp, A., Kröner, A., Proenza, J.A., Lázaro, C., Liu, D., 2016. Recycling and transport of continental material through the mantle wedge above subduction zones: A Caribbean example. Earth and Planetary Science Letters 436, 93-107.

Salters, V.J.M., Stracke, A., 2004. Composition of the depleted mantle. Geochemistry, Geophysics, Geosystems 5, Q05004.

Schmidt, M.W., Poli, S., 2003. Generation of Mobile Components during Subduction of Oceanic Crust. Treatise on Geochemistry 3, 567-591.

Shervais, J.W., 1982. Ti-V plots and the petrogenesis of modern and ophiolitic lavas. Earth and Planetary Science Letters 59, 101-118.

Solari, L.A., Garcia-Casco, A., Martens, U., Lee, J.K.W., Ortega-Rivera, A., 2013. Late Cretaceous subduction of the continental basement of the Maya block (Rabinal Granite, central Guatemala): Tectonic implications for the geodynamic evolution of Central America. Geological Society of America Bulletin 125, 625-639.

Stern, R.J., Bloomer, S.H., 1992. Subduction zone infancy: Examples from the Eocene Izu-Bonin-Mariana and Jurassic California Arcs. GSA Bulletin 104, 1621-1636.

Stern, R.J., Reagan, M., Ishizuka, O., Ohara, Y., Whattam, S., 2012. To understand subduction initiation, study forearc crust: To understand forearc crust, study ophiolites. Lithosphere 4, 469-483.

Su, Y., Langmuir, C.H., 2003. Global MORB Chemistry Compilation at the Segment Scale PhD thesis Department of Earth and Environmental Sciences, Columbia University, New York.

Sun, S.S., McDonough, W.F., 1989. Chemical and isotopic systematics of oceanic basalts: implications for mantle composition and processes, in: Saunders, A.D., Norry, M.J. (Eds.), Magmatism in Ocean Basins. Geological Society of London Special Publications, London, pp. 313–345.

Torró, L., Proenza, J.A., Farré de Pablo, J., Colomer, J.M., Garcia-Casco, A., Melgarejo, J.C., Alfonso, P., Gubern, A., Gallardo, E., Cazañas, X., Chávez, C., del Carpio, R., León, P., Espaillat, J., Lewis, J.F., 2016a. Mineralogy, geochemistry and sulfur isotope characterization of Cerro de Maimón (Dominican Republic), San Fernando and Antonio (Cuba) Lower Cretaceous VMS deposits: Formation during subduction initiation of the Proto-Caribbean lithosphere within a fore-arc. Ore Geology Reviews 72, 794-817.

Torró, L., Garcia-Casco, A., Proenza, J.A., Blanco-Quintero, I.F., Gutiérrez-Alonso, G., Lewis, J.F., 2016b. High-pressure greenschist to blueschist facies transition in the Maimón Formation (Dominican Republic) suggests mid-Cretaceous subduction of the Early Cretaceous Caribbean Arc. Lithos 266-267, 309-331.

Torró, L., Camprubí, A., Proenza, J.A., León, P., Stein, H.J., Lewis, J.F., Nelson, C.E., Chavez, C., Melgarejo, J.C. (accepted). Re-Os and U-Pb geochronology of the Doña Amanda and Cerro Kiosko deposits, Bayaguana district, Dominican Republic: looking down for the porphyry Cu-Mo roots of the Pueblo Viejo-type mineralization in the island-arc tholeiitic series of the Caribbean. Economic Geology (accepted).

Turner, S., Rushmer, T., Reagan, M., Muyen, J.F., 2014. Heading down early on? Start of subduction on Earth. Geology 42, 139-142.

Vila, J.M., Boisson, D., Butterlin, J., Feinburg, H., Pubellier, M., 1987. Le complexe chaotique fini-éocène de Chouchou (Massif du Nord d'Haïti); Un enregistrement du début des décrochements senestres nord-Caraibes. Comptes Rendus de la Académie des Sciences, 304, 39-42.

Walter, M.J., 1998. Melting of garnet peridotite and the origin of komatiite and depleted lithosphere. Journal of Petrology 39, 29–60.

Walter, M.J., 2003. Melt extraction and compositional variability in mantle lithosphere, in: Carlson, R.W. (Ed.), Treatise on Geochemistry, the Mantle and Core, vol2. Elsevier, Amsterdam, pp. 363-394.

Wakabayashi, J., Dilek, Y., 2000. Spatial and temporal relationships between ophiolites and their metamorphic soles: A test of models of forearc ophiolite genesis, in: Dilek, Y., Moores, E.M., Elthon, D., Nicolas, A. (Eds.), Ophiolites and Oceanic Crust: New Insights from Field Studies and the Ocean Drilling Program. Geological Society of America Special Paper 349, 53-64.

Whattam, S.A., Stern, R.J., 2011. The "subduction initiation rule": a key for linking ophiolites, intra-oceanic forearcs, and subduction initiation. Contributions to Mineralogy and Petrology 162, 1031-1045.

Winchester, J.A., Floyd, P.A., 1977. Geochemical discrimination of different magma series and their differentiation products using immobile elements. Chemical Geology 20, 325-343.

Workman, R.K., Hart, S.R., 2005. Major and trace element composition of the depleted MORB mantle (DMM). Earth and Planetary Science Letters 231, 53-72.

Table captions

Table 1: Whole-rock major- and trace-element data for representative volcanic rocks from the Maimón Formation.

Table 2: Nd, Sr and Pb radiogenic isotope compositions of selected igneous rocks from the Maimón Formation.

Figure captions

Figure 1: (a) Geographic location of the boninite and IAT volcanic series (green) and ophiolitic peridotites (black) in the Greater Antilles. Compilation from references in the main text. Abbreviations: EPGFZ: Enriquillo-Plantain Garden fault zone; SFZ: Septentrional fault zone; HFZ: Hispaniola fault zone; BGFZ: Bonao-La Guácara fault zone; SJRFZ: San Juan-Restauración fault zone. (b) Geologic map of the Maimón Fm. in the Cordillera Central of the Dominican Republic (modified from Martín and Draper, 1999) with the locations of the studied samples and the sampled drill hole collars; new detailed 1:5,000 geological mapping of several sectors near the Cerro de Maimón map is included.

Figure 2: Selected element mobility diagrams (major, LILE, transition metals, HFSE and REE) for rocks of the Maimón Fm. Zr/TiO_2 ratios are chosen as a proxy of magmatic evolution trends. The grey arrows indicate the expected magmatic differentiation trends (see Hollis et al., 2014). Our new geochemical data are represented in colour whereas data from Lewis et al. (2000, 2002) and Horan (1995) are drawn in grey. Major and trace element abundances are in wt. % and ppm, respectively.

Figure 3: (a) Zr/Ti vs. Nb/Y (Pearce, 1996 after Winchester and Floyd, 1977) and (b) Th/Co (Hastie et al., 2007) classification diagrams for mafic and felsic volcanic rocks of the Maimón Formation. Compositions of volcanic rocks of the Los Ranchos Fm. (grey areas) (Escuder-Viruete et al., 2006) are shown for comparison.

Figure 4: (a) AFM diagram of Irvine and Baragar (1971) showing the boundary between tholeiitic and calc-alkaline fields; all the (meta)volcanic rocks of the Maimón Formation plot in the tholeiitic field. (b) Fe+Ti-Al-Mg diagram of Jensen (1976) displaying the tholeiitic (TH), calc-alkaline (CA) and komatiitic fields and the lithologies of volcanic rocks; note that all the Maimón rocks plot in the sector of high-Fe tholeiites and that their compositions span from those of basalts to rhyolites. Only the least altered rocks of the Maimón Formation are represented (see the main text; note that Group 1 basalts are not represented since all these specimens are altered beyond the defined threshold). Data of volcanic rocks from the Los Ranchos Formation are from Escuder-Viruete et al. (2006).

Figure 5: Chondrite-normalized REE (a, c and e) and N-MORB-normalized (b, d and f) multi-elemental patterns of basalts and basaltic andesites from the Maimón Formation. Chondrite (C1) values are from McDonough and Sun (1995) and NMORB values from Sun and McDonough

(1989). Geochemical data of samples of the Los Ranchos Formation (LRF) are from Escuder-Viruete et al. (2006). Geochemical data of forearc basalts (FAB), transitional basalts and boninites from Mariana and Izu-Bonin are from Reagan et al. (2010) and Ishizuka et al. (2011), respectively. Symbols as in Figure 2.

Figure 6: Chondrite-normalized REE (a) and N-MORB-normalized (b) multi-elemental patterns of andesites and plagiorhyolites from the Maimón Formation. Chondrite (C1) values are from McDonough and Sun (1995) and NMORB values from Sun and McDonough (1989). Geochemical data of samples of the Los Ranchos Formation (LRF) are from Escuder-Viruete et al. (2006). Symbols as in Figure 2.

Figure 7: Age-corrected (125 Ma) Nd-Sr (a) and Pb (b, c) radiogenic isotope ratios of meta-volcanic whole-rocks of the Maimón Formation. The isotopic compositions of mantle reservoirs (coloured stars) are from Hofmann (2003), Salters and Stracke (2004) and Workman and Hart (2005). Age-corrected (125 Ma) data of IAT series in the Greater Antilles (grey circles) are from: Horan (1995), Escuder-Viruete et al. (2006, 2007a, 2010), Jolly et al. (2008), Marchesi et al. (2007) and Rojas-Agramonte et al. (2016). Present-day Pb isotopic data of the Los Ranchos Fm. in (b, c) (green circles) are from Cumming and Kesler (1987), who did not provide the U, Th, Pb contents of these samples.

Figure 8: Nb/Y vs Th/Yb plot (modified from Pearce and Peate, 1995) for volcanic rocks from the Maimón Formation including the mantle array from depleted (D-DMM) to relatively enriched (E-DMM) mantle sources. DMM (depleted MORB mantle, *average*), D-DMM (depleted DMM) and E-DMM (enriched DMM) after Workman and Hart (2005). Symbols as in Fig. 2; triangles with dot: Group 3i; triangles without dot: Group 3ii (see main text). Geochemical data of the Los Ranchos Formation are from Escuder-Viruete et al. (2006). Geochemical data of forearc basalts (FAB), transitional basalts and boninites from the Izu-Bonin-Mariana (IBM) arc are from Reagan et al. (2010) and Ishizuka et al. (2011), respectively.

Figure 9: Chondrite-normalised Yb versus Sm contents of meta-volcanic rocks of the Maimón Formation compared to values of melts produced by anhydrous and hydrous non-modal fractional melting of depleted MORB mantle (DMM) and depleted DMM (D-DMM) (Workman and Hart, 2005). Anhydrous melting in the spinel lherzolite facies (solid line with black circles) was modelled using source and melting ol:opx:cpx modal proportions = 0.54:0.28:0.18 and -0.11:0.59:0.53, respectively (Niu, 1997 at 1.5 GPa). The solid line with red circles shows the results of 5% anhydrous non-modal fractional melting of DMM in the garnet stability field [source and melting

ol:opx:cpx:grt modal proportions 0.57:0.21:0.13:0.09 and 0.05:-0.15:0.97:0.14, respectively (Walter, 1998 at 3 GPa)] followed by the same melting model in the spinel stability field described above. Modes of the spinel peridotite source after partial melting in the garnet stability field are calculated by the equation of Johnson et al. (1990). Partition coefficients from Bedini and Bodinier (1999), Donnelly et al. (2004) and Su and Langmuir (2003). Hydrous melting in the spinel lherzolite stability field is modelled by 0.03 wt. % stepwise addition of the maximum (solid line with blue circles for DMM or green circles for D-DMM source, respectively) or minimum fluids (dashed line with blue circles for DMM or green circles for D-DMM source, respectively) of Bizimis et al. (2000) at each 0.1% melting increment [melting ol:opx:cpx modal proportions: -0.10:0.52:0.56, Bizimis et al. (2000); partition coefficients of clinopyroxene from Gaetani et al. (2003)]. Symbols as in Figure 2. Labels indicate partial melting degrees and percentages of fluid in the mantle source. Normalising values from Sun and McDonough (1989).

Figure 10: Age-corrected (125 Ma) whole-rock Nd-Sr (a) and Pb (b, c) isotopic ratios of meta-volcanic rocks of the Maimón Formation compared to results of mixing models (solid and dashed lines) between DMM at 125 Ma (green star, Salters and Stracke, 2004; Workman and Hart, 2005) and fluids liberated from Atlantic Cretaceous pelagic sediments (AKPS). Symbols as in Figure 2. Age-corrected isotopic ratios of AKPS (pink circles) are from Jolly et al. (2006). Partition coefficients between metasediments and fluids from Johnson and Plank (1999). Labels indicate the percentages of fluid contribution.

Figure 11: Changes in subduction sensitive elements and ratios between the Maimón LREE-depleted LOTI (Group 1), boninites (Group 2) and normal LOTI (Group 3) basalts. In order to trace temporal lithogeochemical vectors, we assume the lower stratigraphic position of Group 1 basalts observed in drill holes. Data of basalts from the Los Ranchos Formation (Escuder-Viruete et al., 2006) and from the IBM forearc (Ishizuka et al., 2011; Reagan et al., 2010) are given for comparison.

Figure 12: (a) Ti/1000 vs V (ppm) (after Shervais, 1982), (b) Zr (ppm) vs TiO_2 (wt. %), and (c) TiO_2 (wt. %) vs La/Sm plots for basaltic rocks of the Maimón Formation. Symbols as in Fig. 2. Geochemical data of forearc basalts (FAB), transitional basalts and boninites from the Izu-Bonin-Mariana (IBM) arc are after Reagan et al. (2010) and Ishizuka et al. (2011), respectively along with geochemical data for modern arc systems in (c) compiled by Meffre et al. (1996). Geochemical data of the Los Ranchos Formation are from Escuder-Viruete et al. (2006).

Figure 13: Simplified tectonic model for magma generation during subduction initiation beneath the Greater Antilles paleo-arc in the Early Cretaceous. The cartoon is based on the subduction-initiation ophiolite model of Whattam and Stern (2011) adapted to the tectonic reconstruction of the Caribbean region in the Early Cretaceous by Pindell et al. (2012). Approximate ages are based on Escuder-Viruete et al. (2014) and Torró et al. (*accepted*, and references therein). Group 1 Maimón basalts are proposed to form at some stage between the (b) and (c) *snapshots*. Normal IAT volcanism in (d) represents the upper Los Ranchos basaltic unit. Short light blue arrows indicate the flux of fluids/melts from the subducting slab to the mantle wedge. Red arrows mark the directions of mantle flow. Further details are given in the text.

Appendices

Appendix_A: Whole-rock major- and trace-element data for representative volcanic rocks from the Maimón Formation.

Appendix B: Element mobility diagrams (major, LILE, transition metals, HFSE and REE) for rocks of the Maimón Fm. Zr/TiO_2 ratios are chosen as a proxy of magmatic evolution trends. The grey arrows indicate the expected magmatic differentiation patterns. Our new geochemical data are represented in colour whereas data from Lewis et al. (2000, 2002) and Horan (1995) are drawn in grey. Major and trace element abundances are in wt. % and ppm, respectively.

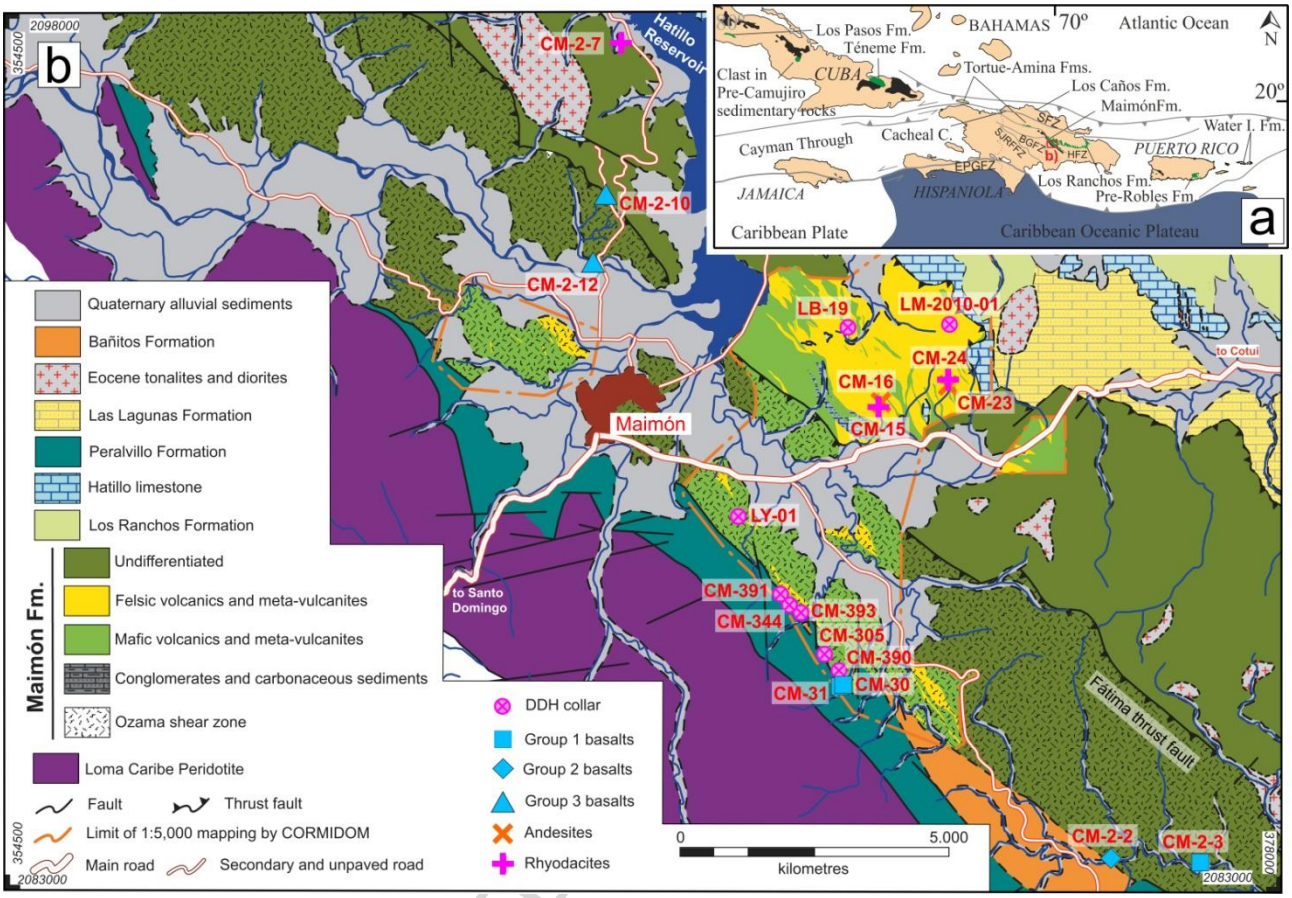

Figure 1

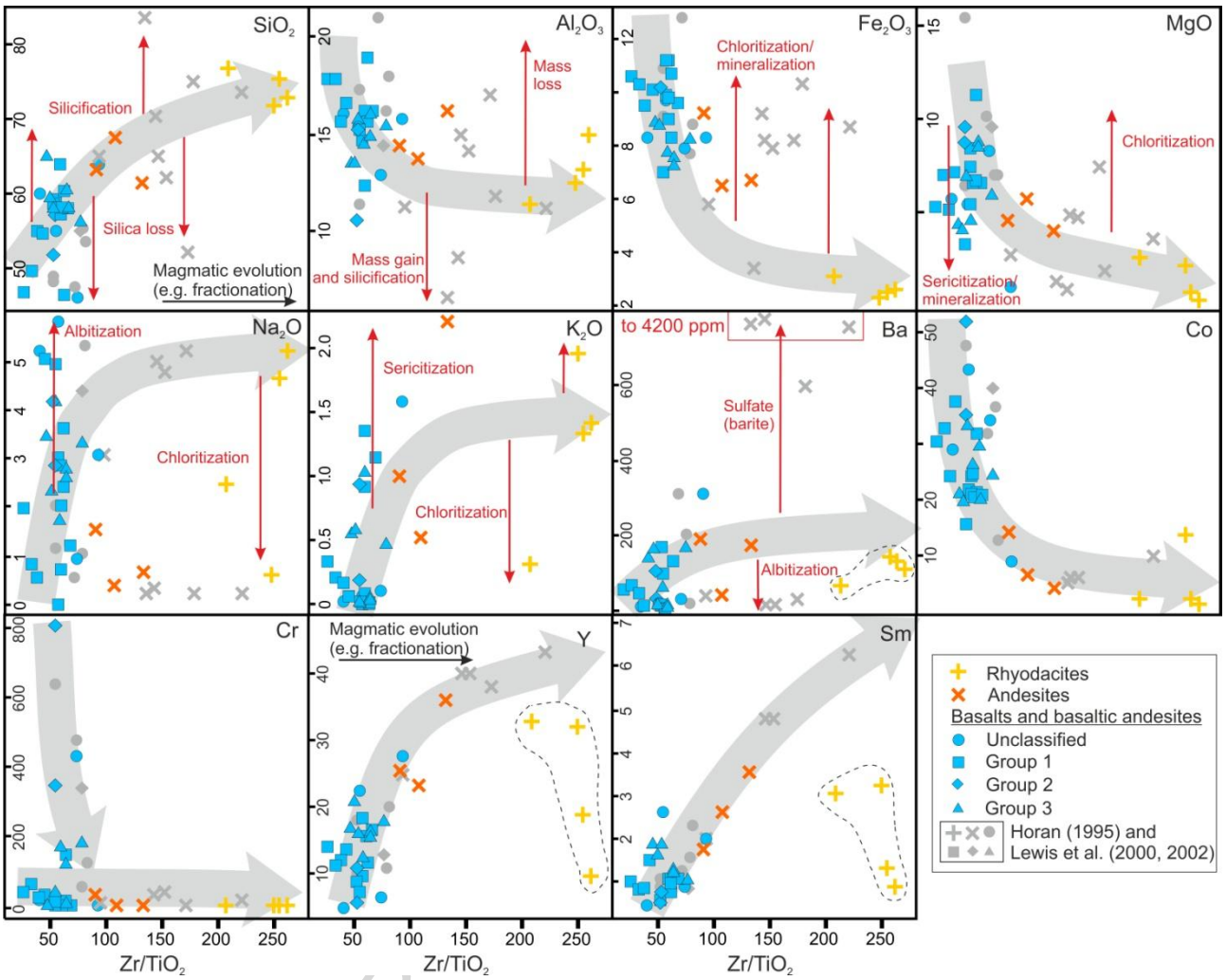

Figure 2

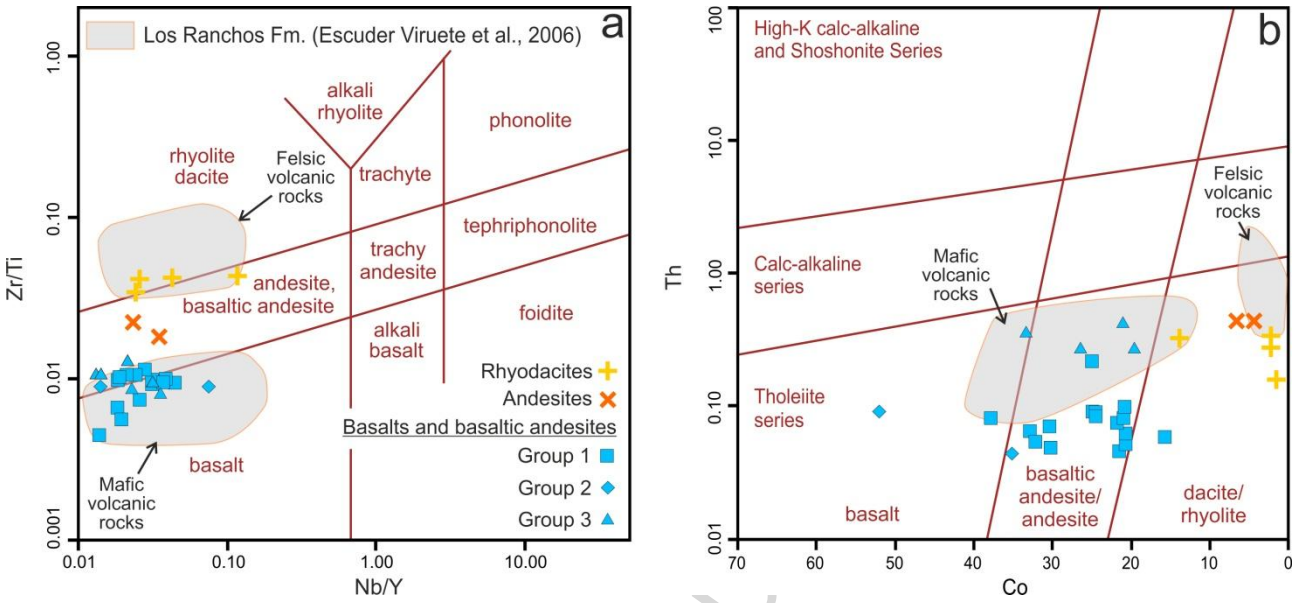

Figure 3

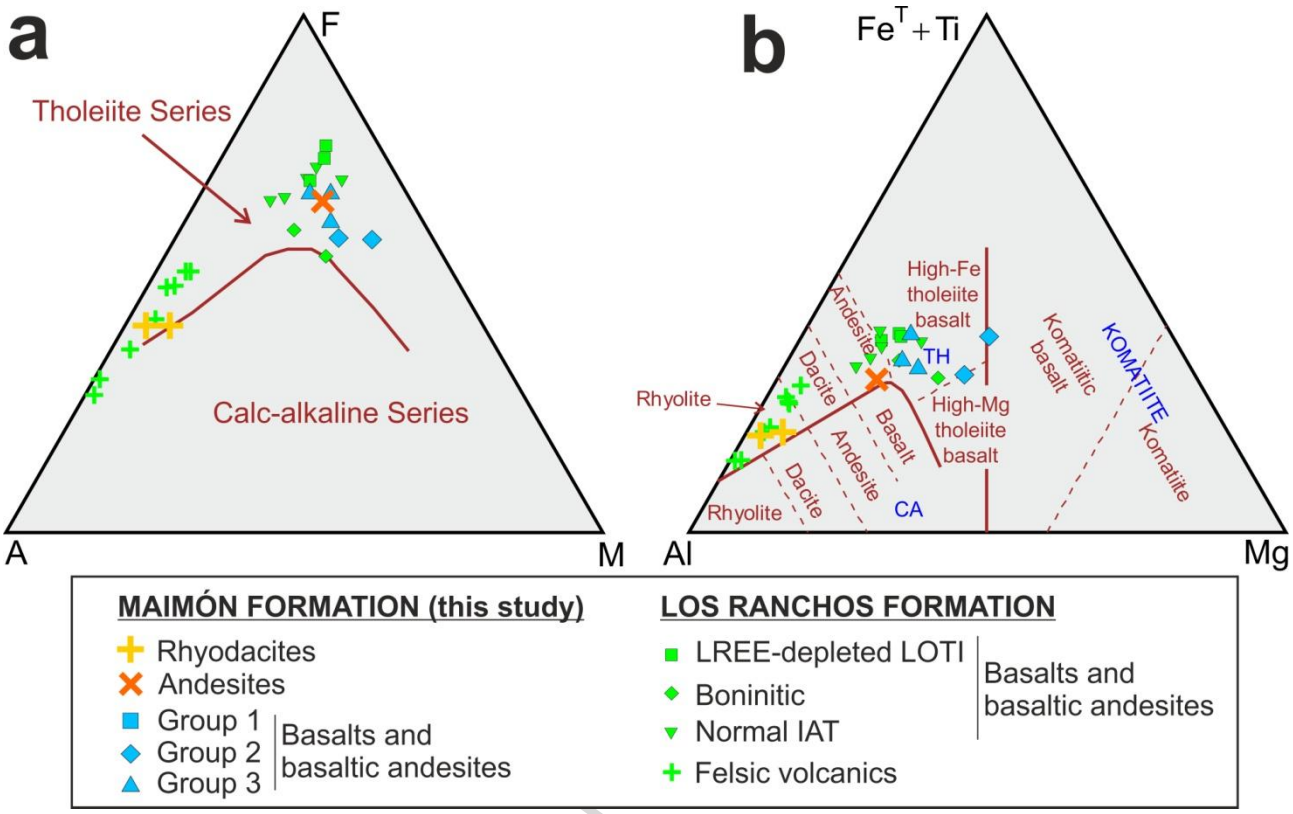

Figure 4

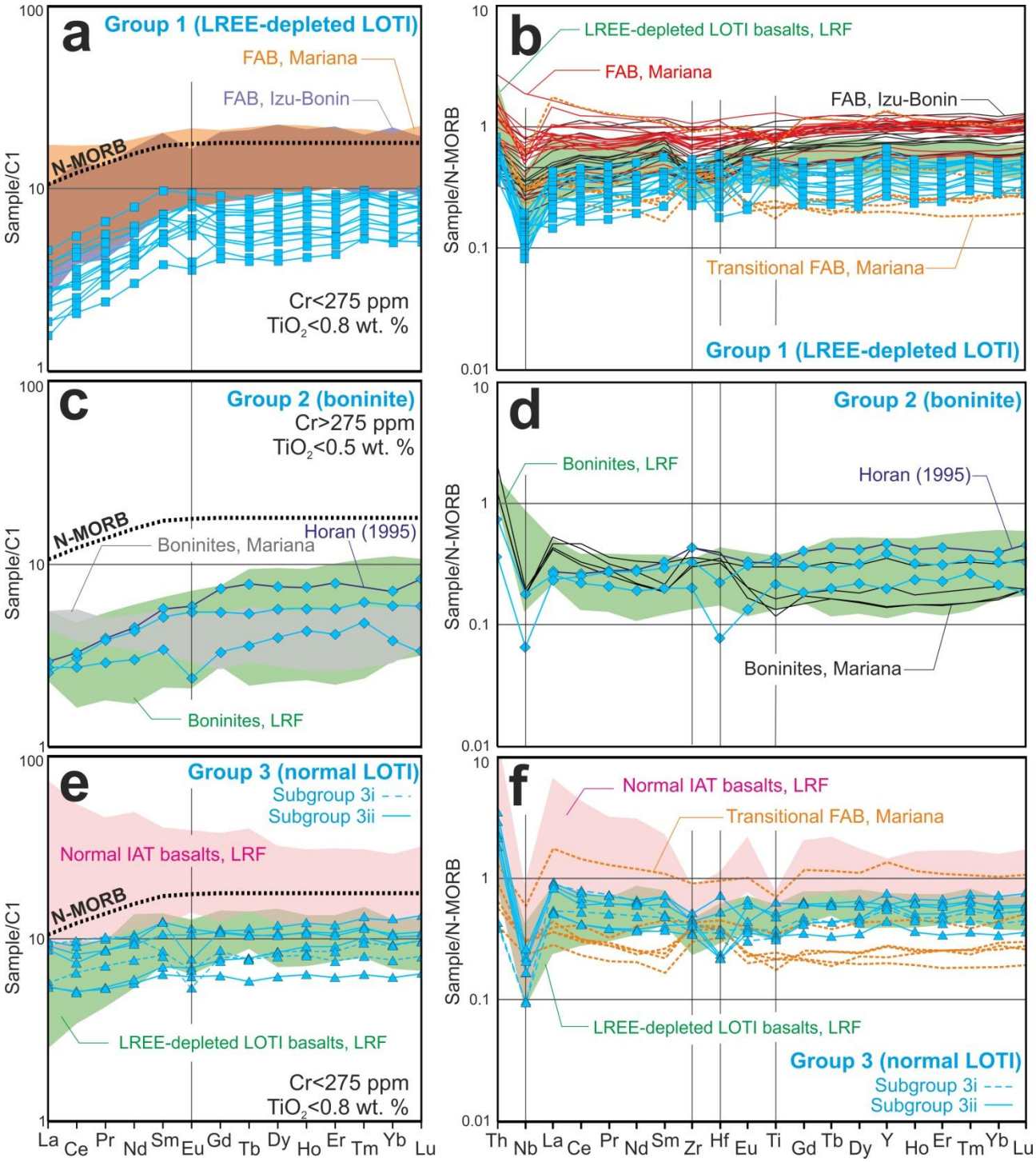
a
Group 1 (LREE-depleted LOTI)
FAB, Mariana
FAB, Izu-Bonin
N-MORB
Cr<275 ppm
TiO2<0.8 wt. %
Sample/C1
b
LREE-depleted LOTI basalts, LRF
FAB, Mariana
FAB, Izu-Bonin
Transitional FAB, Mariana
Group 1 (LREE-depleted LOTI)
Sample/N-MORB
c
Group 2 (boninite)
Cr>275 ppm
TiO2<0.5 wt. %
N-MORB
Boninites, Mariana
Horan (1995)
Boninites, LRF
d
Group 2 (boninite)
Boninites, LRF
Horan (1995)
Boninites, Mariana
e
Group 3 (normal LOTI)
Subgroup 3i
Subgroup 3ii
Normal IAT basalts, LRF
N-MORB
LREE-depleted LOTI basalts, LRF
Cr<275 ppm
TiO2<0.8 wt. %
La Ce Pr Nd Sm Eu Gd Tb Dy Ho Er Tm Yb Lu
f
Normal IAT basalts, LRF
Transitional FAB, Mariana
LREE-depleted LOTI basalts, LRF
Group 3 (normal LOTI)
Subgroup 3i
Subgroup 3ii
Th Nb La Ce Pr Nd Sm Zr Hf Eu Ti Gd Tb Dy Y Ho Er Tm Yb Lu

Figure 5

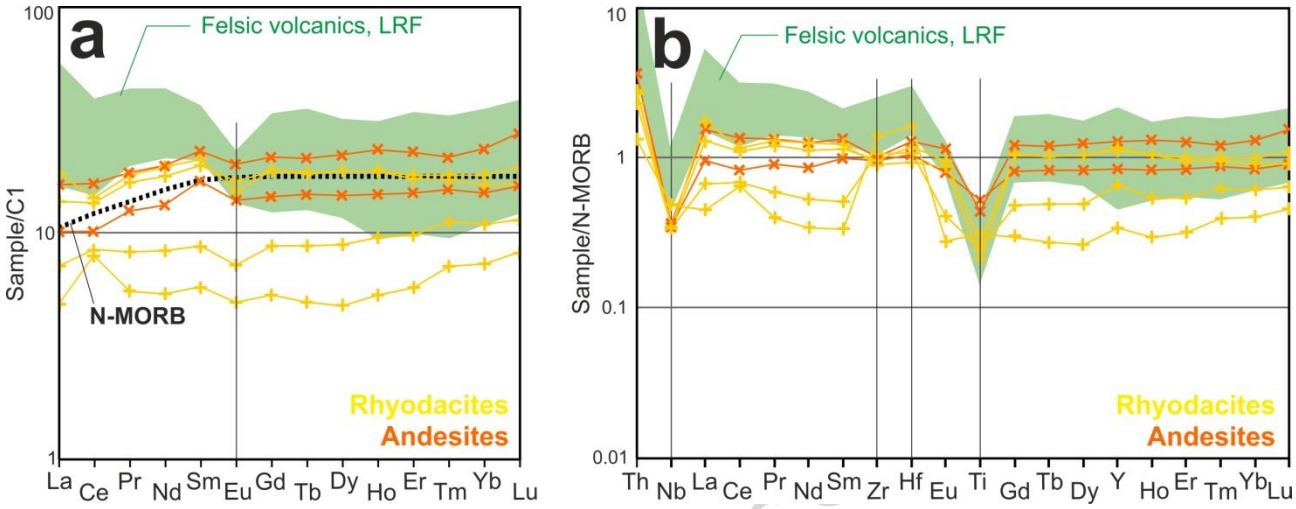

Figure 6

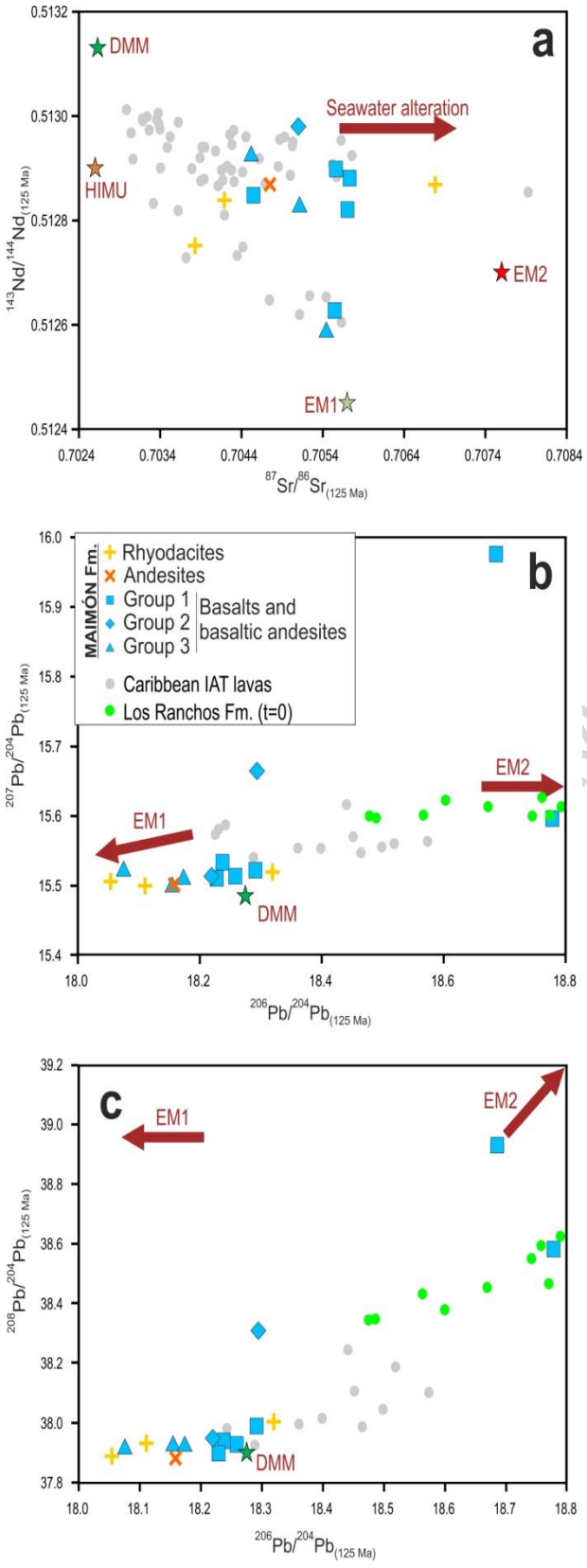

Figure 7

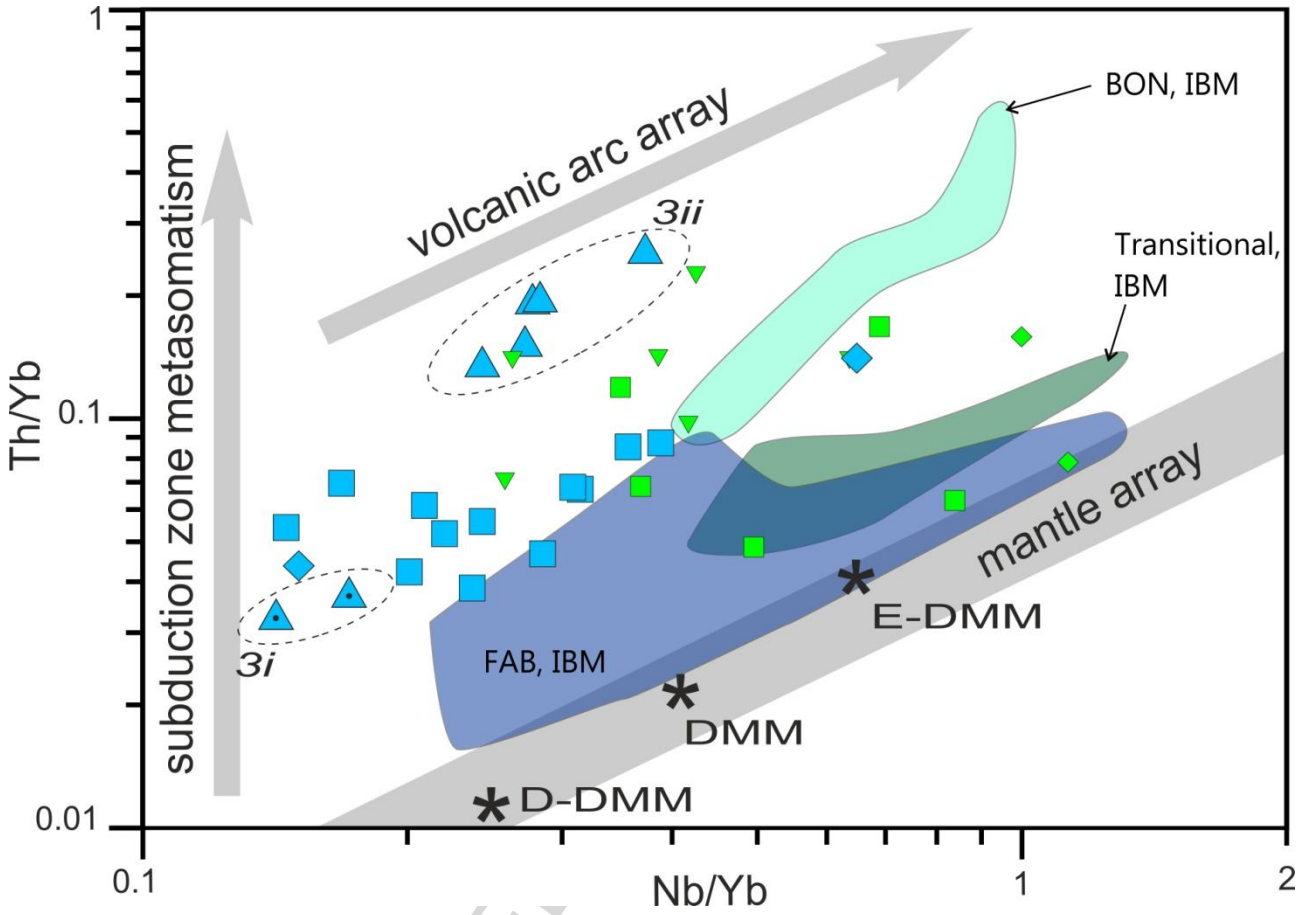

Figure 8

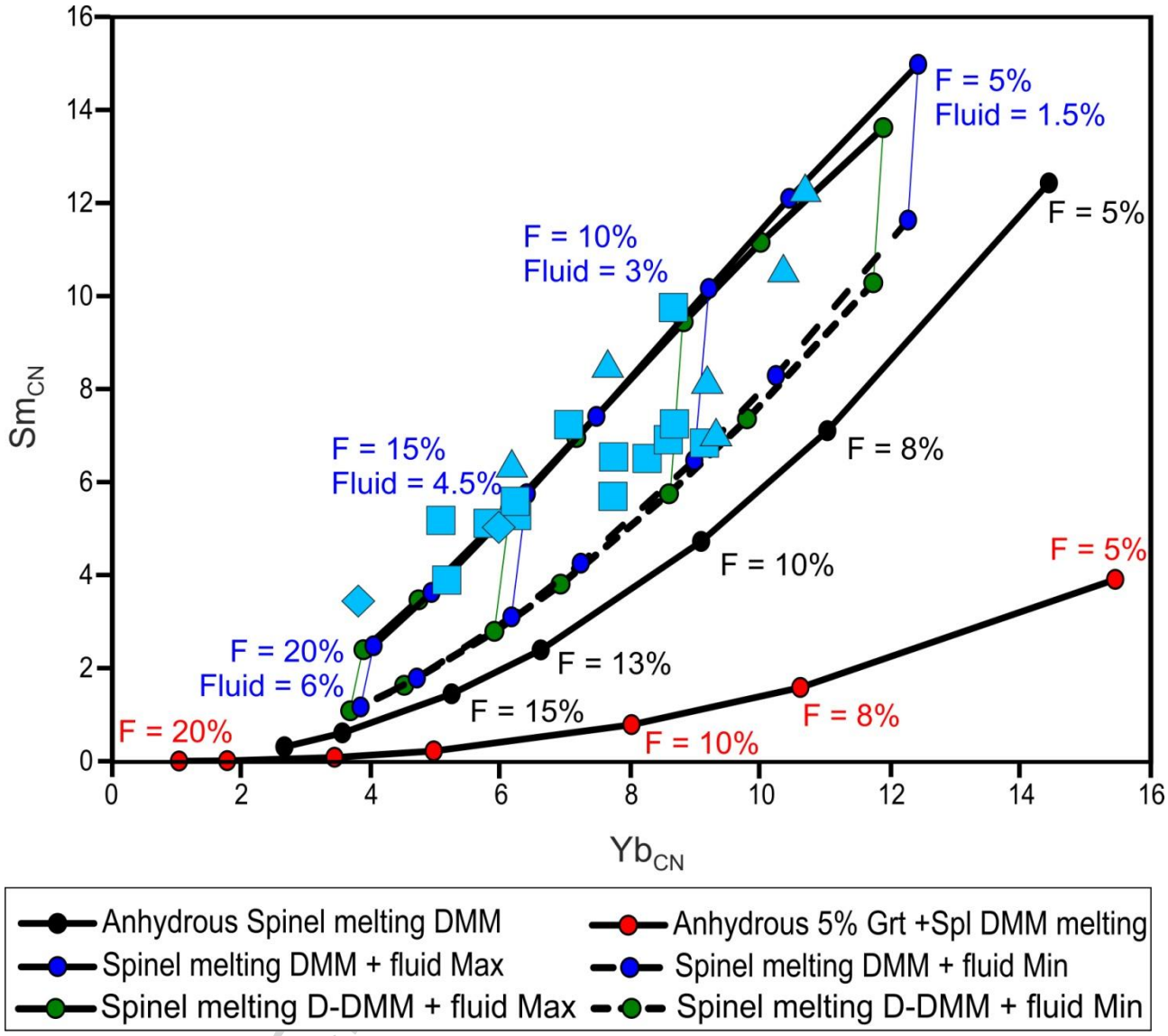

Figure 9

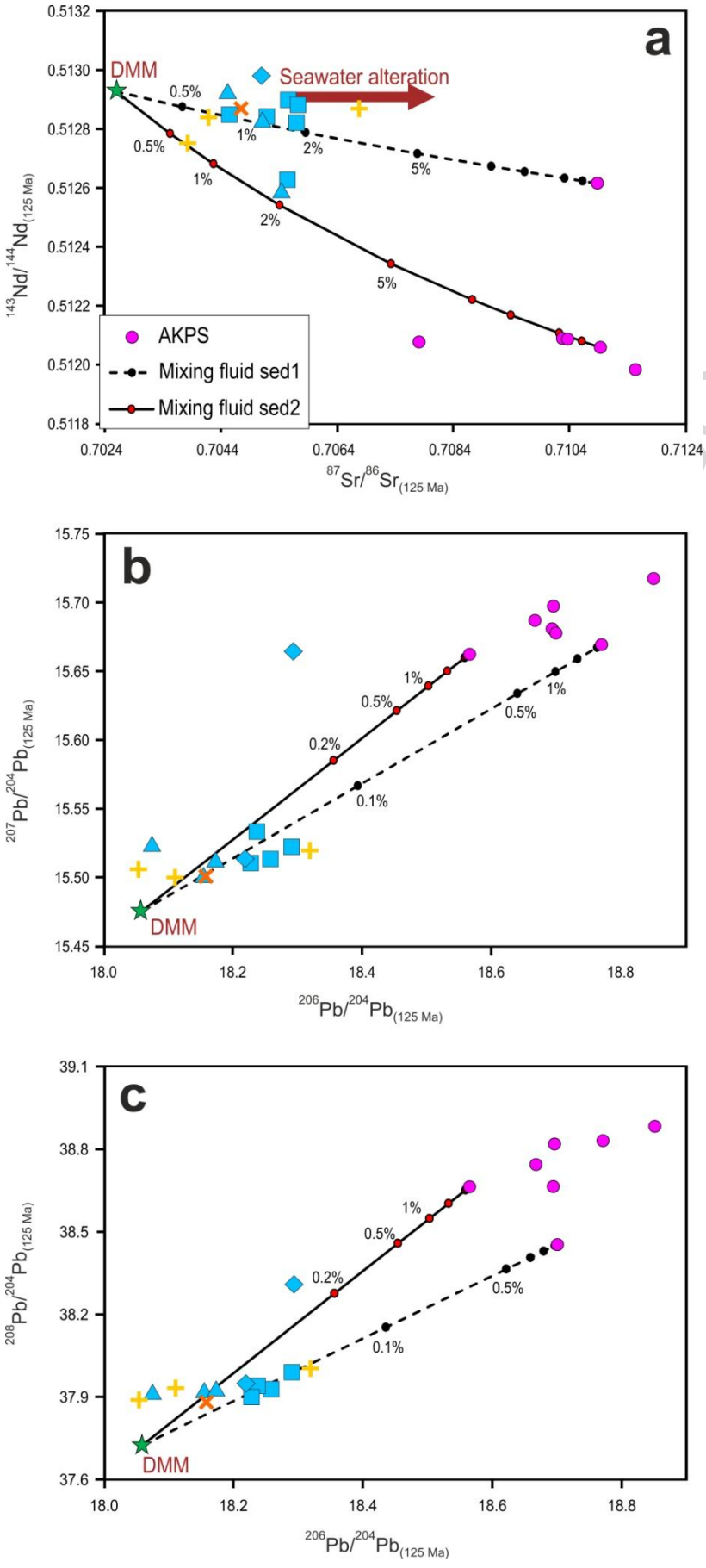

Figure 10

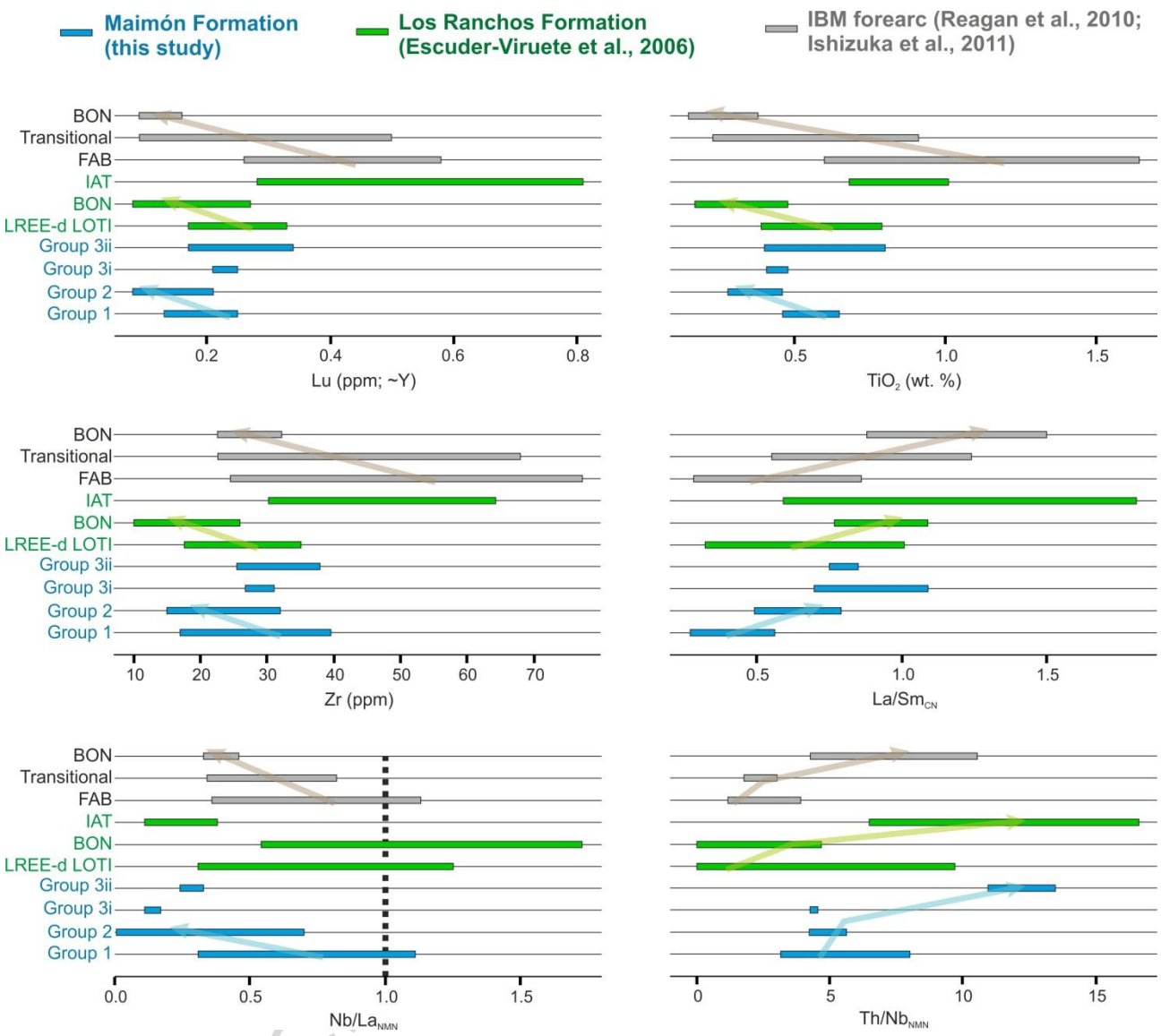

Figure 11

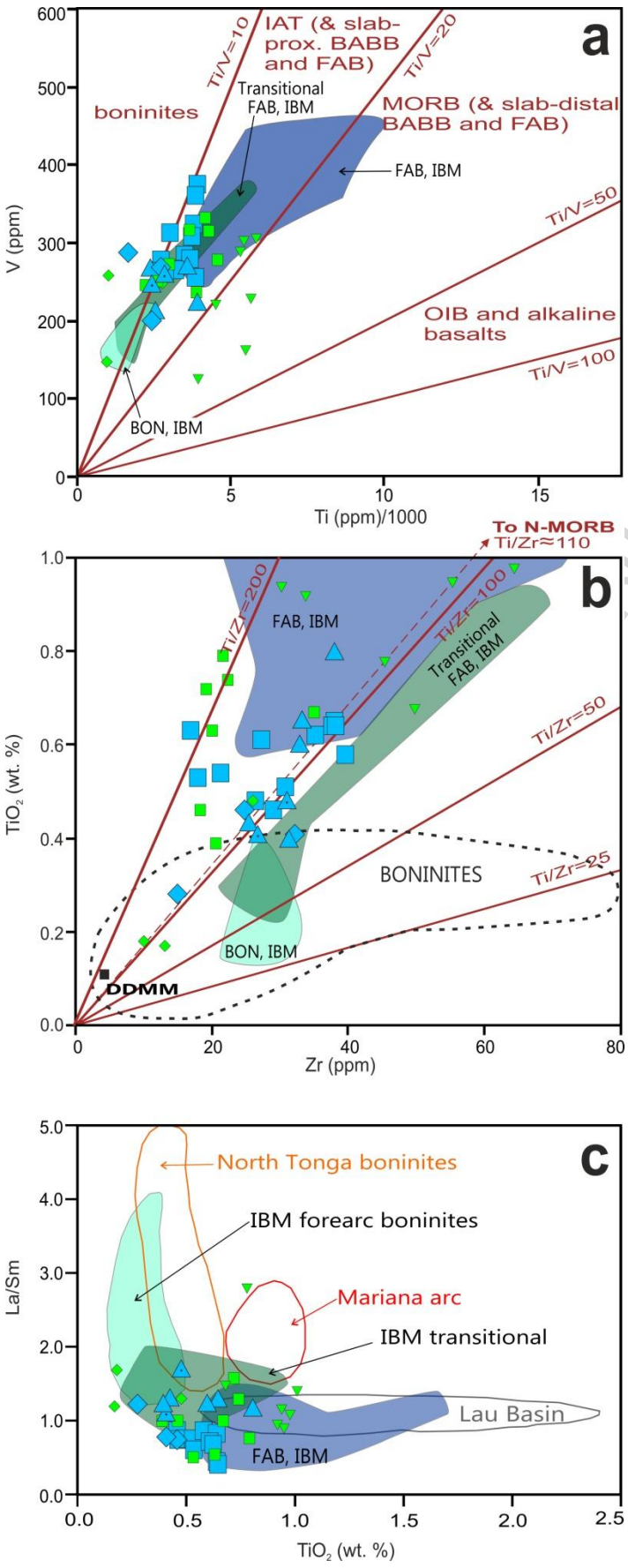

Figure 12

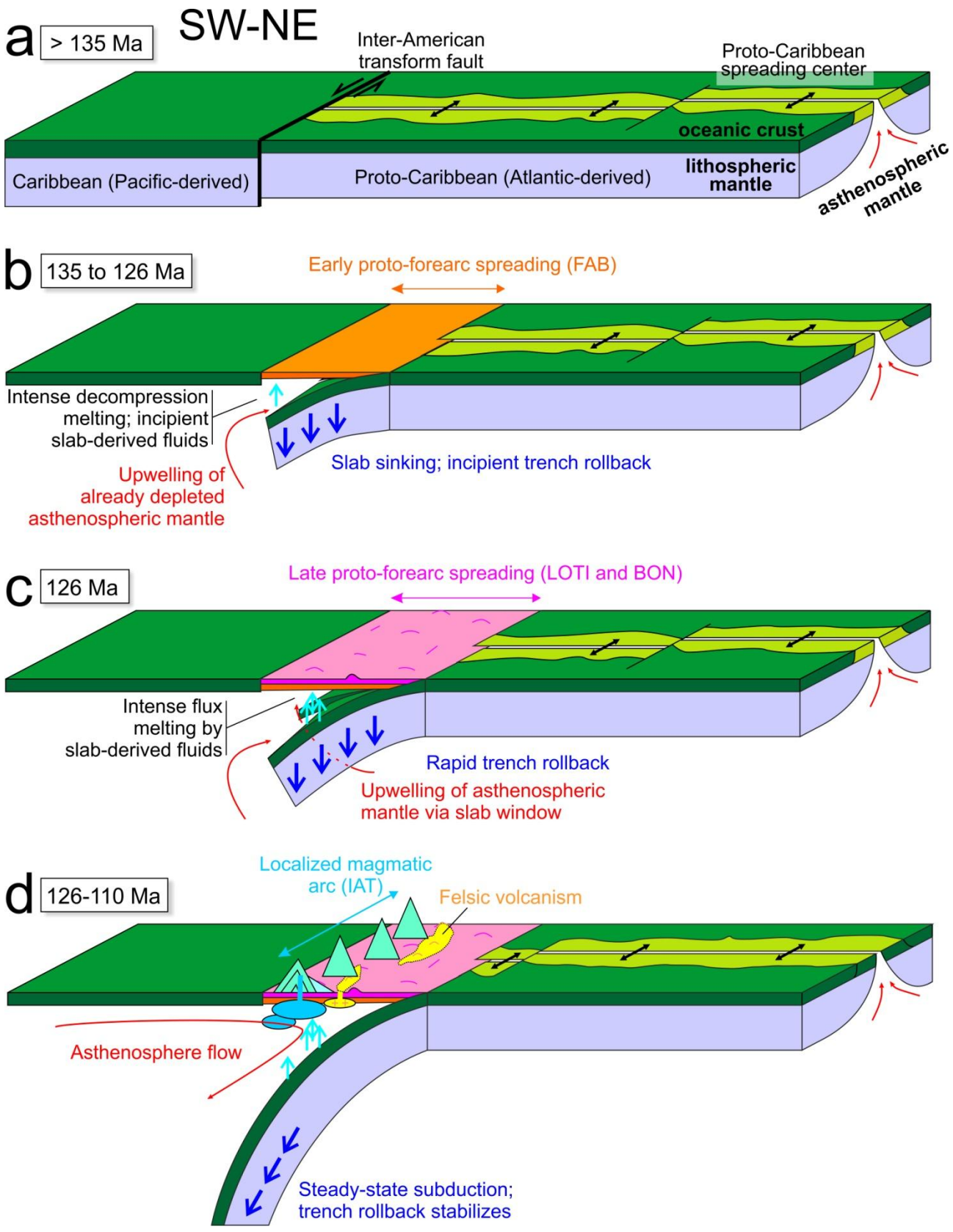

Figure 13

Table 1

Type	Basalts and basaltic andesites										Andesites	Rhyodacites
Group	Group 1				Group 2		Group 3i		Group 3ii			
DDH	Outcrop	Outcrop	CM-305	CM-344	LM-01	Outcrop	CM-344	CM-344	CM-390	Outcrop	Outcrop	LM-01
UTM E	369888	376482	369531	368884	371888	374816	368884	368884	369799	365312	370603	371888
UTM N	2086225	2082949	2086765	2087651	2092667	2083067	2087651	2087651	2086454	2093830	2091261	2092667
Sample	CM-30	CM-2-3	CM-305-10	CM-344-3	LM-01-3	CM-2-2	CM-344-9	CM-344-12	CM-390-11	CM-2-12	CM-16	LM-01-2
wt. %												
SiO_2	54.99	54.72	59.37	58.36	51.72	57.02	60.63	58.33	59.37	64.88	61.48	75.37
Al_2O_3	15.61	16.62	15.68	16.14	15.20	10.61	14.98	16.02	13.50	13.49	16.25	13.22
Fe_2O_3	9.49	10.11	9.89	9.60	9.19	10.15	7.32	7.54	8.74	8.87	6.72	2.52
MnO	0.16	0.21	0.14	0.17	0.17	0.21	0.18	0.21	0.20	0.11	0.06	0.04
MgO	5.16	7.13	6.79	6.55	9.60	8.79	8.58	8.92	4.11	4.38	4.03	0.85
CaO	8.10	1.31	0.13	1.50	7.20	5.72	0.60	0.50	4.69	0.20	4.03	0.55
Na_2O	0.53	5.05	3.04	1.18	2.87	4.18	2.64	2.79	2.32	3.44	0.63	4.67
K_2O	0.15	0.05	0.00	1.14	0.18	0.94	0.03	0.06	0.57	0.54	2.20	1.32
TiO_2	0.54	0.61	0.62	0.58	0.46	0.28	0.48	0.41	0.65	0.80	0.56	0.31
P_2O_5	0.03	0.05	0.03	0.07	0.04	0.03	0.08	0.16	0.06	0.08	0.09	0.07

LOI	4.78	3.77	3.72	4.14	2.85	1.74	4.39	4.37	5.11	2.83	3.30	0.65
Total	99.54	99.63	99.41	99.43	99.48	99.66	99.91	99.31	99.32	99.61	99.35	99.57
ppm												
Li	17.78	6.55	18.24	31.47	6.85	2.63	5.58	5.53	8.10	6.25	36.89	1.90
Rb	2.24	0.99	0.31	9.60	1.44	9.95	0.36	0.78	7.95	3.83	19.27	10.41
Cs	0.12	0.03	0.03	0.10	0.03	0.28	0.02	0.02	0.14	0.09	0.40	0.08
Sr	142.70	39.01	26.54	135.41	49.27	4.84	21.19	20.56	128.86	9.19	358.91	30.60
Ba	44.56	11.05	5.33	129.08	28.20	103.09	13.64	11.13	162.23	138.99	172.07	128.30
Sc	37.58	37.14	29.99	35.74	38.95	41.92	34.51	34.04	32.30	27.42	18.52	8.62
V	264.84	278.95	307.56	283.75	267.70	286.53	258.37	246.83	220.77	51.18	54.61	10.43
Cr	24.47	33.93	3.55	4.88	348.56	806.54	124.18	15.79	9.85	2.12	2.85	1.81
Co	24.38	37.87	21.84	20.83	35.17	52.04	30.21	20.75	19.58	21.09	4.38	2.17
Ni	22.99	19.87	6.54	8.84	108.31	156.04	37.27	26.23	8.03	3.83	2.80	1.14
Cu	85.11	92.04	9.88	66.20	39.70	3.26	29.61	7.02	26.27	60.88	6.62	3.61
Zn	67.83	81.71	145.75	134.87	49.57	109.46	117.41	145.04	80.66	171.16	76.98	35.65
Ga	13.97	15.82	15.04	15.30	12.83	13.34	12.74	13.10	12.46	15.40	16.68	11.39
Y	12.03	13.85	7.45	16.31	10.86	5.52	15.80	16.52	20.76	16.83	35.91	18.72
Nb	0.22	0.36	0.33	0.46	0.15	0.42	0.22	0.22	0.48	0.60	0.85	0.80

Ta	0.04	0.11	0.05	0.05	0.04	0.11	0.04	0.04	0.06	0.08	0.08	0.06
Zr	21.3	27.3	35.2	39.5	24.8	15.0	31.0	26.7	33.2	38.0	74.4	78.6
Hf	0.69	0.46	0.85	1.21	0.47	0.16	0.77	0.73	0.48	1.47	2.64	2.22
Pb	0.92	1.22	1.65	5.12	1.15	0.93	1.60	3.86	1.84	2.02	5.43	2.40
U	0.09	0.08	0.10	0.32	0.03	0.01	0.16	0.14	0.17	0.51	0.22	0.22
Th	0.09	0.08	0.08	0.10	0.04	0.09	0.05	0.05	0.27	0.42	0.44	0.28
La	0.54	1.07	0.59	0.92	0.59	0.65	2.21	1.36	2.08	2.18	3.88	1.69
Ce	1.57	3.40	1.99	2.78	1.87	1.66	6.02	4.02	4.51	5.04	10.11	5.17
Pr	0.33	0.63	0.38	0.49	0.36	0.27	0.97	0.68	0.83	0.82	1.76	0.79
Nd	1.80	3.71	2.17	2.73	2.00	1.40	4.73	3.59	4.34	4.52	9.26	3.90
Sm	0.87	1.49	0.79	1.06	0.78	0.53	1.31	1.25	1.62	1.89	3.53	1.34
Eu	0.40	0.55	0.36	0.38	0.32	0.14	0.39	0.31	0.61	0.45	1.17	0.42
Gd	1.25	1.89	0.93	1.55	1.12	0.68	1.77	1.63	2.24	2.29	4.47	1.80
Tb	0.24	0.33	0.16	0.28	0.20	0.13	0.29	0.29	0.40	0.42	0.81	0.33
Dy	1.68	2.38	1.02	1.96	1.44	1.01	2.05	2.17	2.65	2.97	5.69	2.26
Ho	0.40	0.54	0.24	0.46	0.33	0.24	0.46	0.48	0.62	0.69	1.33	0.54
Er	1.14	1.47	0.72	1.36	0.94	0.68	1.26	1.42	1.79	1.98	3.79	1.62
Tm	0.22	0.25	0.14	0.23	0.16	0.12	0.21	0.24	0.30	0.33	0.55	0.29

Yb	1.31	1.47	0.86	1.46	1.01	0.65	1.30	1.56	1.76	2.16	4.01	1.87
Lu	0.21	0.20	0.15	0.24	0.15	0.08	0.21	0.25	0.27	0.34	0.70	0.29

[1]DDH refers to the identification of the Diamanond Drill Holes from which the samples were collected; surface samples are identified as "outcrop".

[2]For DDH samples, and coordinates refer to the location of collars. UTM Zone 19 (NAD27 for US).

Table 2

Sample	Rock type	Group	$^{87}Sr/^{86}Sr$	$^{87}Sr/^{86}Sr$ (125 Ma)	$^{143}Nd/^{144}Nd$	$^{143}Nd/^{144}Nd$ (125 Ma)	εNd (125 Ma)	$^{206}Pb/^{204}Pb$	$^{206}Pb/^{204}Pb$ (125 Ma)	$^{207}Pb/^{204}Pb$	$^{207}Pb/^{204}Pb$ (125 Ma)	$^{208}Pb/^{204}Pb$	$^{208}Pb/^{204}Pb$ (125 Ma)
LM-01-3	Basalt	1	0.70525 ± 28	0.705100	0.513173 ± 15	0.512979	9.8	18.2534 ± 10	18.2197	15.5151 ± 10	15.5134	37.9645 ± 27	37.9492
CM-2-2	Basalt	1	0.710102 ± 21	-	0.512886 ± 15	0.512700	4.6	18.3126 ± 18	18.2942	15.6651 ± 16	15.6642	38.3484 ± 42	38.3090
LY-01-15	Basalt	2	0.705748 ± 28	0.705729	0.513088 ± 15	0.512881	7.9	18.2713 ± 8	18.2376	15.5349 ± 8	15.5332	37.9541 ± 20	37.9404
CM-2-3	Basalt	2	0.704677 ± 28	0.704546	0.513047 ± 21	0.512848	7.3	18.7704 ± 27	18.6855	15.9795 ± 24	15.9753	38.9580 ± 59	38.9303
CM-305-01	Basalt	2	0.705283 ± 21	0.705192	0.513078 ± 15	0.512841	7.4	18.8316 ± 14	18.7776	15.5986 ± 12	15.5960	38.6082 ± 32	38.5824
LY-01-14	Basalt	2	0.705773 ± 21	0.705704	0.513028 ± 15	0.512821	6.9	18.3432 ± 13	18.2915	15.5246 ± 11	15.5221	38.0051 ± 30	37.9901
CM-390-14	Basalt	2	0.705607 ± 21	0.705560	0.513101 ± 15	0.512898	8.4	18.3082 ± 12	18.2587	15.5156 ± 10	15.5132	37.9439 ± 28	37.9281
CM-390-15	Basalt	2	0.705564 ± 21	0.705546	0.512836 ± 15	0.512627	3.2	18.2731 ±14	18.2283	15.5125 ± 12	15.5103	37.9123 ± 33	37.8992
GII-2-4	Basalt	3ii	0.704668 ± 21	0.704518	0.513109 ± 15	0.512928	8.5	18.2596 ± 8	18.1737	15.5170 ± 7	15.5128	37.9898 ± 18	37.9308
CM-2-10	Basalt	3ii	0.705538 ± 21	0.705443	0.512782 ± 15	0.512591	2.4	18.2533 ± 7	18.0757	15.5330 ± 6	15.5243	37.9632 ± 18	37.9183

GII-2-3	Basalt 3ii	0.705381 ± 28	0.705114	0.513022 ± 21	0.512831	7.2	18.2259 ± 11	18.1553	15.5050 ± 10	15.5015	37.9597 ± 26	37.9246
CM-16	Andesite	0.705025 ± 14	0.704749	0.513057 ± 15	0.512868	7.9	18.2085 ± 8	18.1586	15.5031 ± 7	15.5007	37.9136 ± 18	37.8813
CM-15	Rhyodacite	0.705303 ± 28	0.703830	0.512927 ± 26	0.512751	5.7	18.2192 ± 9	18.1109	15.5050 ± 8	15.4997	37.9615 ± 21	37.9318
LM-01-2	Rhyodacite	0.705939 ± 28	0.704191	0.513009 ± 15	0.512839	7.1	18.4334 ± 10	18.3196	15.5250 ± 9	15.5194	38.0496 ± 26	38.0034
CM-24	Rhyodacite	0.707124 ± 21	0.706783	0.513049 ± 15	0.512868	7.8	18.2739 ± 11	18.0546	15.5166 ± 10	15.5059	38.0006 ± 25	37.8889

Petrogenesis of meta-volcanic rocks from the Maimón Formation (Dominican Republic): Geochemical record of the nascent Greater Antilles paleo-arc

HIGHLIGHTS

- Petrogenesis of the most primitive arc volcanism in the Caribbean.
- Chemostratigraphic relations indicate progression from FAB-like to boninite and IAT magmas.
- Geochemical evolution mirrors that of subduction-initiation ophiolites.
- Likely genetic connection with adjacent Loma Caribe peridotites.
- Hot subduction of young warm Proto-Caribbean oceanic lithosphere and ridge.